Heterogeneous Optimized Schwarz Methods for Second Order Elliptic PDEs

Gander, Martin Jakob; Vanzan, Tommaso

How to cite

GANDER, Martin Jakob, VANZAN, Tommaso. Heterogeneous Optimized Schwarz Methods for Second Order Elliptic PDEs. In: SIAM journal on scientific computing, 2019, vol. 41, n° 4, p. A2329–A2354. doi: 10.1137/18M122114X

This publication URL: https://archive-ouverte.unige.ch//unige:168646
Publication DOI: 10.1137/18M122114X

SIAM J. SCI. COMPUT.
Vol. 41, No. 4, pp. A2329–A2354

HETEROGENEOUS OPTIMIZED SCHWARZ METHODS FOR SECOND ORDER ELLIPTIC PDES*

MARTIN J. GANDER† AND TOMMASO VANZAN†

Abstract. Due to their property of convergence in the absence of overlap, optimized Schwarz methods are the natural domain decomposition framework for heterogeneous problems, where the spatial decomposition is provided by the multiphysics of the phenomena. We study here heterogeneous problems which arise from the coupling of second order elliptic PDEs. Theoretical results and asymptotic formulas are proposed solving the corresponding min-max problems both for single and double sided optimizations, while numerical results confirm the effectiveness of our approach even when analytical conclusions are not available. Our analysis shows that optimized Schwarz methods do not suffer the heterogeneity, it is the opposite, they are faster the stronger the heterogeneity is. It is even possible to have h independent convergence choosing two independent Robin parameters. This property was proved for a Laplace equation with discontinuous coefficients, but only conjectured for more general couplings in [M. J. Gander and O. Dubois, *Numer. Algorithms*, 69 (2015), pp. 109–144]. Our study is completed by an application to a contaminant transport problem.

Key words. optimized Schwarz methods, heterogeneous domain decomposition methods, optimized transmission conditions, contaminant transport

AMS subject classifications. 65N55, 65N22, 65F10, 65F08

DOI. 10.1137/18M122114X

1. Introduction.

The classical Schwarz method is a domain decomposition algorithm for solving large scale PDEs. It consists of dividing the domain of computation into many subdomains, solving iteratively the local problems while exchanging information along the interfaces through Dirichlet boundary conditions. The pioneering paper [25], in which Lions proposed a convergent algorithm using Robin transmission conditions, paved the way for the development of the optimized Schwarz methods which exploit optimized transmission conditions in order to overcome some of the drawbacks of the classical Schwarz method such as slow convergence and overlap requirement [10]. The procedure to obtain such optimized transmission conditions is now well established [9]: the problem of interest is posed in a simplified setting where one can use the Fourier transform, for unbounded domains, or Fourier series expansion or more generally separation of variables [19, 18], for bounded domains, to transform the PDE into a set of ODEs parametrized by the frequencies k. Then, solving the ODEs and using the transmission conditions, one can get a recursive relation for the Fourier coefficients and obtain a closed formula for the convergence factor which contains some free parameters to optimize.

The literature regarding optimized Schwarz methods for homogeneous problems is well developed. Optimized transmission conditions have been obtained for many problems such as Helmholtz equations [16, 14], Maxwell equations [4, 22, 30], advection diffusion problems [8, 18], Navier–Stokes equations [3], shallow water equations [27], and Euler equations [6]. In all of the previous works, homogeneous problems are analyzed, in the sense that a unique physics is considered in the whole domain, and

*Submitted to the journal's Methods and Algorithms for Scientific Computing section October 16, 2018; accepted for publication (in revised form) March 18, 2019; published electronically July 25, 2019.

https://doi.org/10.1137/18M122114X

†Section de mathématiques, Université de Genève, Genève, CH-1211, Switzerland (martin.gander@unige.ch, tommaso.vanzan@unige.ch).

therefore, the coupling on the interfaces regards equations of the same nature. First attempts to generalize this situation have been carried out in [26, 12], where Laplace equations with different diffusion coefficients were considered, and in [5], which was devoted to Maxwell equations with discontinuous coefficients. Let us remark that at least two possible interpretations of heterogeneous domain decomposition methods exist. The first one concerns problems where the same physical phenomenon is taking place in the whole domain, but it can be convenient to use a cheaper approximation in some parts of the domain in order to save computational resources. This might be the case in the presence of boundary layers, or, for example, in computational fluid dynamics (CFD) simulations where a potential flow is used far away from the zone of interest while the Navier–Stokes equations are fully solved near, for instance, an aircraft. In this situation, good transmission conditions can be obtained through a factorization approach, see [15] for further details.

In this manuscript we follow the second interpretation which assumes that two different physical phenomena are present in the domain and they interact through an interface. In this case some physical coupling conditions must be satisfied along the common interface, such as the continuity of the function and its normal derivative for second order PDEs, or the continuity of normal stresses for fluid-structure problems. Some examples in this direction can be found in [17], where optimized transmission conditions were obtained for the coupling between the hard-to-solve Helmholtz equation and the Laplace equation, or in [21] where a partial optimization procedure was carried out for a fluid-structure problem. For these kinds of heterogeneous problems, a domain decomposition approach can be extremely useful since it allows one to reuse specific solvers designed for the different physics phenomena present in the domain. For instance, one can use a finite volume solver where a strong advection is present while using a multigrid solver where diffusion dominates or an ad-hoc linear elasticity solver combined with a CFD code for the Navier–Stokes equations. In this perspective, optimized Schwarz methods lead to a significantly better convergence of the coupling routine with respect to other domain decomposition algorithms (e.g., Dirichlet–Neumann, Robin–Neumann) since they take into account the physical properties in their transmission conditions. We refer the interested reader to [23, 24] for the application of optimized Schwarz methods for the coupling of atmospheric and oceanic computational simulation models.

We study here first the coupling between a reaction diffusion equation and a diffusion equation and second the harder coupling between a general second order PDE and a reaction diffusion equation. We provide theoretical results and asymptotic formulas for the optimized parameters, and we show the effectiveness through numerical simulations. The manuscript is completed by the application of our results to a physical model describing contaminant transport in underground media, which is a topic of great interest in the last thirty years due, for instance, to the increasing threat of contamination of groundwater supplies by waste treatments and landfill sites or to the disposal of nuclear radioactive waste [2]. We refer to [1] for a reference regarding modeling issues of contaminant transport. Our model assumes that the computational domain $\Omega = \Omega_1 \cup \Omega_2 \cup \Omega_3 \cup \Omega_4$, represented in Figure 1, can be partitioned into four layers. In the first one, the contaminant, whose concentration is described through the unknown u, penetrates mainly thanks to rainfalls and, therefore, an advection towards the negative y direction is present. The next two layers are formed by porous media so that the contaminant spreads in a diffusive regime described by the Laplace equation. Furthermore we suppose that in the second layer, some chemical reactions may take place which are synthesized in the reaction term. Finally, in the

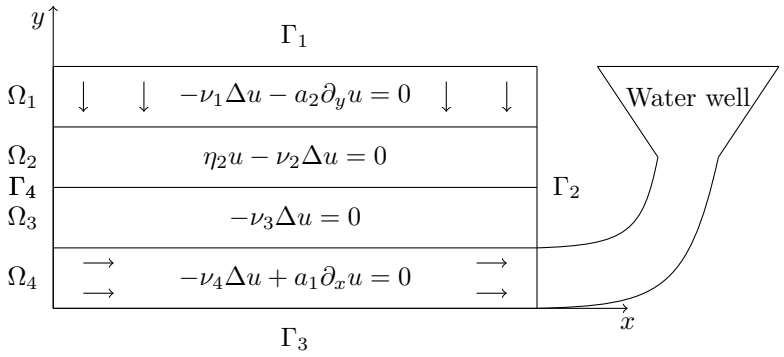

FIG. 1. *Geometry for the contaminant transport problem.*

last layer, an underground flow transports the contaminant in the x direction towards a groundwater supply which is connected to a water well. The problem belongs to the heterogeneous class, since in different parts of the domain we have different physical phenomena, and thus in the last paragraph we use the results discussed in this manuscript to design an efficient domain decomposition method to compute the stationary and time dependent distribution of the contaminant.

2. Reaction diffusion-diffusion coupling. Let us consider two domains $\Omega_1 := (-\infty, 0) \times (0, L)$ and $\Omega_2 := (0, +\infty) \times (0, L)$ and the interface $\Gamma := \{0\} \times (0, L)$. In this section we study a reaction-diffusion equation with discontinuous coefficients along the interface Γ,

$$(\eta^2(x) - \nu(x)\Delta)u = f \quad \text{in} \quad \Omega, \tag{2.1}$$

where $\Omega := \Omega_1 \cup \Omega_2$, $\eta^2(x) = \eta^2 \geq 0$ in Ω_1, and $\eta(x) = 0$ in Ω_2, while $\nu(x) = \nu_1$ in Ω_1 and $\nu(x) = \nu_2$ in Ω_2, with $\nu_1, \nu_2 \in \mathbb{R}^+$. Equation (2.1) is closed by homogeneous Dirichlet boundary conditions on the horizontal edges and assuming $\lim_{x\to\pm\infty} u = 0$. The optimized Schwarz method for this problem is

$$\begin{aligned} (\eta^2 - \nu_1\Delta)u_1^n = f \ \text{ in } \ \Omega_1, \quad (\nu_1\partial_x + S_1)(u_1^n)(0,\cdot) = (\nu_2\partial_x + S_1)(u_2^{n-1})(0,\cdot), \\ -\nu_2\Delta u_2^n = f \ \text{ in } \ \Omega_2, \quad (\nu_2\partial_x - S_2)(u_2^n)(0,\cdot) = (\nu_1\partial_x - S_2)(u_1^{n-1})(0,\cdot), \end{aligned}$$

where S_j, $j = 1, 2$ are linear operators along the interface Γ in the y direction. The goal is to find which operators guarantee the best performance in terms of convergence speed. We consider the error equation whose unknowns are $e_i^n := u_{|\Omega_i} - u_i^n$, $i = 1, 2$, and we expand the solutions in the Fourier basis in the y direction, $e_i^n = \sum_{k\in\mathcal{V}} \hat{e}_i^n(x,k)\sin(ky), i = 1, 2$ with $\mathcal{V} := \left\{\frac{\pi}{L}, \frac{2\pi}{L}, \dots\right\}$. Moreover, we suppose that the operator S_j are diagonalizable, with eigenvectors $\psi_k(y) := \sin(ky)$, such that $S_j\psi_k = \sigma_j(k)\psi_k$, where $\sigma_j(k)$ are the eigenvalues of S_j. Under these assumptions, we find that the coefficients $\hat{e}_i^n$ satisfy

$$\begin{aligned} (\eta^2 - \nu_1\partial_{xx} + \nu_1 k^2)(\hat{e}_1^n) &= 0, && k \in \mathcal{V},\ x < 0, \\ (\nu_1\partial_x + \sigma_1(k))(\hat{e}_1^n)(0,k) &= (\nu_2\partial_x + \sigma_1(k))(\hat{e}_2^{n-1})(0,k), && k \in \mathcal{V}, \\ (-\nu_2\partial_{xx} + \nu_2 k^2)(\hat{e}_2^n) &= 0, && k \in \mathcal{V},\ x > 0, \\ (\nu_2\partial_x - \sigma_2(k))(\hat{e}_2^n)(0,k) &= (\nu_1\partial_x - \sigma_2(k))(\hat{e}_1^{n-1})(0,k), && k \in \mathcal{V}. \end{aligned} \tag{2.2}$$

Solving the two differential equations parametrized by k in (2.2), imposing that the solutions remain bounded for $x \to \pm\infty$ and defining $\lambda(k) := \sqrt{k^2 + \tilde{\eta}^2}$ and $\gamma(k) := k$,

we obtain

$$\begin{aligned} \hat{e}_1^n &= \hat{e}_1^n(0,k)e^{\sqrt{k^2+\tilde{\eta}^2}x} = \hat{e}_1^n(0,k)e^{\lambda(k)x} \quad \text{in} \quad \Omega_1, \\ \hat{e}_2^n &= \hat{e}_2^n(0,k)e^{-kx} = \hat{e}_2^n(0,k)e^{-\gamma(k)x} \quad \text{in} \quad \Omega_2, \end{aligned} \tag{2.3}$$

where $\tilde{\eta}^2 = \frac{\eta^2}{\nu_1}$. The transmission conditions in (2.2) allow us to express the Fourier coefficient at iteration n of the solution in one subdomain as a function of the coefficient of the solution in the other subdomain at the previous iteration $n-1$, namely

$$\hat{e}_1^n(0,k) = \frac{-\nu_2\gamma(k)+\sigma_1(k)}{\nu_1\lambda(k)+\sigma_1(k)}\hat{e}_2^{n-1}(0,k) \tag{2.4}$$

and

$$\hat{e}_2^n(0,k) = \frac{\nu_1\lambda(k)-\sigma_2(k)}{-\nu_2\gamma(k)-\sigma_2(k)}\hat{e}_1^{n-1}(0,k). \tag{2.5}$$

Combining (2.4) and (2.5) we get

$$\hat{e}_1^n(0,k) = \frac{-\nu_2\gamma(k)+\sigma_1(k)}{\nu_1\lambda(k)+\sigma_1(k)} \cdot \frac{\nu_1\lambda(k)-\sigma_2(k)}{-\nu_2\gamma(k)-\sigma_2(k)}\hat{e}_1^{n-2}(0,k).$$

By induction we then obtain

$$\hat{e}_1^{2n}(0,k) = \rho^n\hat{e}_1^0(0,k) \qquad \hat{e}_2^{2n}(0,k) = \rho^n\hat{e}_2^0(0,k),$$

where the convergence factor ρ is defined by

$$\rho := \rho(k,\sigma_1,\sigma_2) = \frac{-\nu_2\gamma(k)+\sigma_1(k)}{\nu_1\lambda(k)+\sigma_1(k)} \cdot \frac{\nu_1\lambda(k)-\sigma_2(k)}{-\nu_2\gamma(k)-\sigma_2(k)}.$$

Expressing the dependence on the Fourier frequency k we get

$$\rho(k,\sigma_1,\sigma_2) = \frac{-\nu_2 k+\sigma_1(k)}{\nu_1\sqrt{k^2+\tilde{\eta}^2}+\sigma_1(k)} \cdot \frac{\nu_1\sqrt{k^2+\tilde{\eta}^2}-\sigma_2(k)}{-\nu_2 k-\sigma_2(k)}. \tag{2.6}$$

A closer inspection of (2.6) leads us to conclude that if we chose the operators S_j such that their eigenvalues are

$$\sigma_1^{\text{opt}}(k) := \nu_2 k \quad \text{and} \quad \sigma_2^{\text{opt}}(k) := \nu_1\sqrt{k^2+\tilde{\eta}^2}, \tag{2.7}$$

then we would have $\rho \equiv 0$. In this case the algorithm would converge in just two iterations. This option, even though it is optimal, leads to nonlocal operators S_j^{opt}, which correspond to the Schur complements [29], and they are expensive from the computational point of view. Indeed, the operator associated with the eigenvalues $\sigma_1^{\text{opt}}(k) := \nu_2 k$ corresponds to the square root of the Laplacian on the interface Γ, i.e., $S_1^{\text{opt}} = \nu_2(-\Delta_\Gamma)^{\frac{1}{2}}$, which is a fractional and nonlocal operator. The nonlocal property of S_1^{opt} can also be understood considering a discretization of the straight interface Γ and the discrete counterpart of S_1^{opt}, i.e., $S_{1h}^{\text{opt}} := \nu_2(-\Delta_{y,h})^{\frac{1}{2}}$, where $-\Delta_{y,h} = \text{diag}(-1,2,-1)$ is the classical one-dimensional Laplacian. A direct implementation shows that the matrix S_{1h}^{opt} is dense. Even though the use of S_{1h}^{opt} would destroy the sparsity of the subdomain matrices, theoretically it could still be used as a transmission condition and the method would then converge in two iterations.

However, the major drawback is that, in general, we do not know the operator S_j^{opt} and, therefore, we would have to assemble numerically the Schur complements. This is an operation which requires the knowledge of the inverse of the subdomain operators and therefore it is computationally expensive.

We thus look for classes of convenient transmission conditions which are amenable to easy implementation, and then to find which transmission conditions among a specific class lead to the best convergence factor. We consider here zeroth order approximations of the optimal operators in (2.7) which correspond to classical Robin conditions on the interface. In order to get the best transmission conditions in terms of convergence speed, we have to minimize the maximum of the convergence factor over all the frequencies k. Defining $\mathcal{D}_1, \mathcal{D}_2$ as the classes of transmission conditions, we are looking for a couple $(\sigma_1^*, \sigma_2^*) \in \mathcal{D} := \mathcal{D}_1 \times \mathcal{D}_2$ such that

$$(\sigma_1^*, \sigma_2^*) = \underset{(\sigma_1,\sigma_2)\in\mathcal{D}}{\arg\min} \Big(\max_{k_{\min}\le k\le k_{\max}} |\rho(k, \sigma_1, \sigma_2)| \Big). \tag{2.8}$$

The lower and upper bounds $k_{\min}$, $k_{\max}$ depend on the problem under study: $k_{\min}$ is given by the Fourier expansion and here it is equal to $k_{\min} = \frac{\pi}{L}$. The presence of $k_{\min}$ in (2.8), is the "memory" that our problem has of the boundedness of the domain; see [11, 20, 19] for more details on the influence of the domain for optimized Schwarz methods. The upper bound $k_{\max}$ is instead the maximum frequency that can be resolved by the grid and it is typically estimated as $k_{\max} = \frac{\pi}{h}$ where h is a measure of the grid spacing.

2.1. Zeroth order single sided optimized transmission conditions. Let p be a free parameter, we define

$$\sigma_1(k) = \nu_2 p, \quad \sigma_2(k) = \nu_1 \sqrt{\tilde{\eta}^2 + p^2}. \tag{2.9}$$

We have made this choice because the optimal operators in (2.7) are clearly rescaled according to the diffusion constants of the two subdomains, and thus we imitate this behavior. Furthermore, we introduce the parameter $\tilde{\eta}^2$ in the definition of $\sigma_2(k)$ in order to make the problem amenable to analytical treatment. With this choice, we have $\sigma_j(k) = \sigma_j^{opt}(k)$ for $k = p$; in other words, for the frequency $k = p$, the transmission conditions lead to an exact solver which converges in two iterations. The idea of introducing free parameters such that the eigenvalues $\sigma_j(k)$ are identical to the optimal ones for a certain frequency is essential because, as we will see in the following, it allows us to solve the min-max problems which, for a generic choice of σ_j, are extremely hard to solve.

Inserting the expressions (2.9) into (2.6), the min-max problem (2.8) becomes

$$\min_{p\in\mathbb{R}} \max_{k_{\min}\le k\le k_{\max}} \left| \frac{k-p}{k+\lambda\sqrt{p^2+\tilde{\eta}^2}} \cdot \frac{\sqrt{k^2+\tilde{\eta}^2} - \sqrt{p^2+\tilde{\eta}^2}}{\sqrt{k^2+\tilde{\eta}^2} + \frac{p}{\lambda}} \right|, \tag{2.10}$$

where $\lambda = \frac{\nu_1}{\nu_2}$. We define

$$\rho(k,p) := \frac{k-p}{k+\lambda\sqrt{p^2+\tilde{\eta}^2}} \cdot \frac{\sqrt{k^2+\tilde{\eta}^2} - \sqrt{p^2+\tilde{\eta}^2}}{\sqrt{k^2+\tilde{\eta}^2} + \frac{p}{\lambda}}.$$

We are now solving the min-max problem (2.10). The main steps are the following:

- Restricting the range in which we are searching for p.

- Identifying the candidates for the maxima in the variable k.
- Studying how the maxima behave when varying the parameter p.

LEMMA 2.1 (restriction for the interval of p). *If p^* is a solution to problem (2.10), then p^* belongs to the interval $[k_{\min}, k_{\max}]$.*

Proof. First, we note that $|\rho(k,p)| < |\rho(k,-p)|$ for every $p \geq 0$. Therefore, we can assume $p^* \in \mathbb{R}^+$. Moreover, the function is always positive and equal to zero only for $k = p$. Thus, we can neglect the absolute value. Direct calculations show that $\frac{\partial \rho(k,p)}{\partial p} = h(k,p)$, where

(2.11)
$$h(k,p) := \frac{(p-k)\lambda p(\sqrt{k^2+\tilde{\eta}^2}\lambda + k)}{(k+\lambda\sqrt{p^2+\tilde{\eta}^2})^2(\sqrt{k^2+\tilde{\eta}^2}\lambda + p)\sqrt{p^2+\tilde{\eta}^2}} + \frac{(\sqrt{p^2+\tilde{\eta}^2} - \sqrt{k^2+\tilde{\eta}^2})\lambda(\sqrt{k^2+\tilde{\eta}^2}\lambda + k)}{(k+\lambda\sqrt{p^2+\tilde{\eta}^2})(\sqrt{k^2+\tilde{\eta}^2}\lambda + p)^2}.$$

We observe that if $p^* < k_{\min}$, then $\frac{\partial \rho}{\partial p}(k,p^*) < 0$ for all $k \in [k_{\min}, k_{\max}]$, hence we are certainly not at the optimum since increasing p^* would decrease the convergence factor for all the frequencies $k \in [k_{\min}, k_{\max}]$.

On the other hand, if $p^* > k_{\max}$, then we have $\frac{\partial \rho}{\partial p}(k,p^*) > 0 \ \forall k \in [k_{\min}, k_{\max}]$. Hence we cannot be at the optimum either since decreasing p^* would decrease $\rho(k,p)$ $\forall k \in [k_{\min}, k_{\max}]$. Thus we can conclude that if p^* is a solution of (2.10), then p^* lies in the interval $[k_{\min}, k_{\max}]$. ∎

Now we focus on the search of the maxima of $\rho(p,k)$ with respect to k keeping in mind that p belongs to $[k_{\min}, k_{\max}]$.

LEMMA 2.2 (local maxima in k). *For any fixed value of $p \in [k_{\min}, k_{\max}]$, the function $k \to \rho(k,p)$ assumes its maximum either at $k = k_{\min}$ or at $k = k_{\max}$.*

Proof. We consider the derivative of $\rho(k,p)$ with respect to k and we remind that $\rho(k,p)$ is always positive so we may neglect the absolute value. Direct calculations show that $\frac{\partial \rho}{\partial k} = h(p,k)$. Thus considering (2.11) we have that letting $p \in (k_{\min}, k_{\max})$, $\frac{\partial \rho}{\partial k} < 0 \ \forall k < p$, and $\frac{\partial \rho}{\partial k} > 0 \ \forall k > p$. Therefore, the maximum is attained on the boundary, either at $k = k_{\min}$ or $k = k_{\max}$.

On the other hand, if $p = k_{\min}$, $\rho(k, k_{\min})$ has a zero in $k = k_{\min}$. For all of the other values of k in the interval $[k_{\min}, k_{\max}]$, the function is strictly increasing and, therefore, the maximum is attained at $k = k_{\max}$. The case $p = k_{\max}$ is identical and hence the result follows. ∎

We now have all of the ingredients needed to solve the min-max problem (2.10).

THEOREM 2.3. *The unique optimized Robin parameter p^* solving the min-max problem (2.10) is given by the unique root of the nonlinear equation*

$$|\rho(k_{\min}, p^*)| = |\rho(k_{\max}, p^*)|. \tag{2.12}$$

Proof. From the previous lemmas, we know that we can rewrite problem (2.10) as

$$\min_{p \in [k_{\min}, k_{\max}]} \max \left\{ \rho(k_{\min}, p), \rho(k_{\max}, p) \right\},$$

i.e. the maximum is either attained at $k = k_{\min}$ or $k = k_{\max}$. We now show that the optimal p^* satisfies a classical equioscillation property [32]; see Figure 2 for a graphical representation. We first note that $\rho(k_{\min}, p) = 0$ for $p = k_{\min}$, and $\frac{\partial \rho(k_{\min},p)}{\partial p} > 0 \ \forall p \in (k_{\min}, k_{\max}]$. Therefore, increasing p, $\rho(k_{\min}, p)$ strictly increases until it reaches its maximum value for $p = k_{\max}$. On the other hand, we have that $\rho(k_{\max}, k_{\min})$ is strictly greater than zero, and while p increases from $k_{\min}$ to $k_{\max}$, $\rho(k_{\max}, p)$ decreases, being $\frac{\partial \rho(k_{\max},p)}{\partial p} < 0 \ \forall p \in [k_{\min}, k_{\max})$. Furthermore, we have that $\rho(k_{\max}, k_{\max}) = 0$.

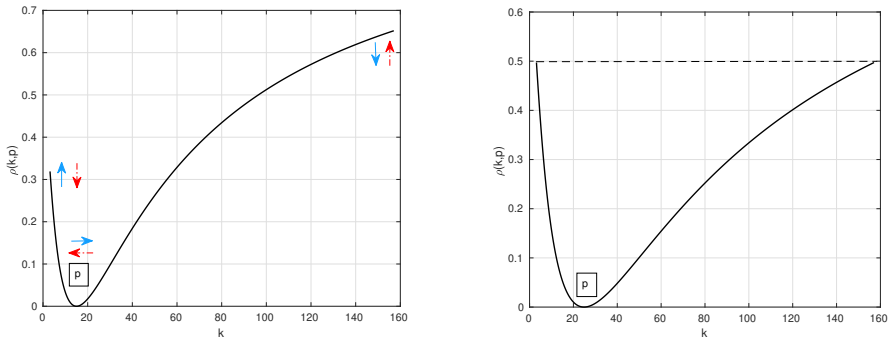

FIG. 2. *Illustration of the equioscillation property described in Theorem* 2.3.

Hence, thanks to the strict monotonicity of both $\rho(k_{\min}, p)$ and $\rho(k_{\max}, p)$, there exists by continuity a unique value p^* such that $\rho(k_{\min}, p^*) = \rho(k_{\max}, p^*)$. This value is clearly the optimum, because perturbing p^* would increase the value of ρ at one of the two extrema and, therefore, the maximum of ρ over all k. ∎

Even though a closed form solution of (2.12) is not known, it is interesting to study asymptotically how the algorithm performs. Therefore, we keep ν_1, ν_2, and $\tilde{\eta}^2$ fixed, and $k_{\max} = \frac{\pi}{h}$ while letting $h \to 0$. This is a case of interest since usually we want to decrease the mesh size h in order to get a better approximation and, therefore, it is useful to see how the method performs in this regime. We introduce the notation $f(h) \sim g(h)$ as $h \to 0$ if and only if $\lim_{h\to 0} \frac{f(h)}{g(h)} = 1$.

THEOREM 2.4. *Let* $D := \sqrt{k_{\min}^2 + \tilde{\eta}^2}$. *Then if* $\nu_1, \nu_2, \tilde{\eta}^2$ *are kept fixed,* $k_{\max} = \frac{\pi}{h}$ *and* h *is small enough, then the optimized Robin parameter* p^* *is given by*

$$p^* \sim C \cdot h^{-\frac{1}{2}}, \quad C := \sqrt{\frac{(\lambda D + k_{\min})\pi}{(\lambda + 1)}}. \tag{2.13}$$

Furthermore, the asymptotic convergence factor of the heterogeneous optimized Schwarz method is

$$\max_{k_{\min} \le k \le \pi/h} |\rho(k, p^*)| \sim 1 - h^{\frac{1}{2}} \left[\frac{\lambda D}{C} + \frac{D}{C} + \frac{k_{\min}}{\lambda C} + \frac{k_{\min}}{C} \right]. \tag{2.14}$$

Proof. We make the ansatz $p = C \cdot h^{-\alpha}$ in (2.12). Expanding for small h, we get that

$$|\rho(k_{\min}, p)| \sim 1 - h^{\alpha} \left[\frac{\lambda D}{C} + \frac{D}{C} + \frac{k_{\min}}{\lambda C} + \frac{k_{\min}}{C} \right].$$

On the other hand,

$$|\rho(k_{\max}, p)| \sim 1 - h^{1-\alpha} \left[\frac{\lambda C}{\pi} + \frac{2C}{\pi} + \frac{C}{\lambda \pi} \right].$$

Comparing the first two terms we get the result. ∎

Remark 2.5. Note that if we set $\tilde{\eta}^2 = 0$, then we recover the results for the coupling of two Laplace equations with different diffusion constants; see [12]. In that

TABLE 1
Comparison between the optimal solution p^* of Theorem 2.3 and the optimal solution $\bar{p}$ computed numerically for the min-max problem involving $\sigma_1(k) = \nu_2 p$ and $\sigma_2(k) = \nu_1 p$. Mesh size equal to $h = \frac{1}{50}$.

$\tilde{\eta}$	p^*	$\bar{p}$	$\max_k \rho(k, p^*)$	$\max_k \rho(k, \bar{p})$
1	22.47	22.47	0.5618	0.5618
100	72.11	110.09	0.0737	0.0452
500	92.21	508.2691	0.0025	0.0081
1000	95	1005	$3.74 \cdot 10^{-4}$	0.0026

case,

$$\rho \sim 1 - h^{\frac{1}{2}} \sqrt{\frac{k_{\min}}{\pi}} \left[\frac{(\lambda+1)^2}{\lambda} \right], \qquad p^* = \sqrt{k_{\min}\pi} h^{-\frac{1}{2}}.$$

Moreover, we have that the convergence factor (2.14) satisfies for $\lambda = \frac{\nu_1}{\nu_2} \to \infty$, $|\rho| \sim 1 - h^{\frac{1}{2}} \lambda \sqrt{\frac{D}{\pi}}$ and for $\lambda \to 0$, $|\rho| \sim 1 - h^{\frac{1}{2}} \frac{1}{\lambda} \sqrt{\frac{k_{\min}}{\pi}}$. On the other hand, as $\tilde{\eta} \to \infty$ we have $|\rho| \sim 1 - h^{\frac{1}{2}} \sqrt{\tilde{\eta}} \frac{(\lambda+1)^{\frac{3}{2}}}{\sqrt{\lambda\pi}}$. It follows that for all strong heterogeneity limits, the constant in front of the asymptotic term $h^{\frac{1}{2}}$ becomes larger; therefore, the deterioration is slower and the method is more efficient.

Remark 2.6. One could object that if we set $\sigma_1(k) = \nu_2 p$ and $\sigma_2(k) = \nu_1 p$, without introducing the ad-hoc term involving $\tilde{\eta}$ in the definition $\sigma_2(k)$, it may be possible to improve the method. In this case the convergence factor would have two zeros, one located at $k_1 := p$ and the other one located in $k_2 := \sqrt{p^2 - \tilde{\eta}^2}$. The min-max problem is then much harder to solve analytically because one of the zeros depends on the parameter p in a nonlinear way. Furthermore, for $p < \tilde{\eta}$ the second zero is not real, for values of p slightly larger, than $\tilde{\eta}$, the distance between the two zeros might be significant while if p is very large then $k_1 \approx k_2$. A large number of different cases arises which makes the min-max problem really hard to solve. However, even though we are unable to solve the min-max problem for a general setting of parameters, it is possible to draw conclusions in the case in which $k_{\max}$ is large enough. In fact from an analysis of the convergence factor we deduce that $\rho(k_{\max}, p) \to 1$ as $h \to 0$. If we impose equioscillation between $\rho(k_{\min}, p)$ and $\rho(k_{\max}, p)$, calculations show that then p goes to infinity as $h \to 0$ and, therefore, we have three local maxima in the interval $[k_{\min}, k_{\max}]$, two at the boundary and an interior maximum, $\hat{k}$ located between the two zeros. Estimating asymptotically $|\rho(\hat{k}, p)|$ as $h \to 0$ using the convexity of the function in the interval $[k_1, k_2]$, we obtain

$$|\rho(\hat{k}, p)| \leq \frac{\partial \rho}{\partial k}|_{(k=\sqrt{p^2-\tilde{\eta}^2}, p)} \cdot |p - \sqrt{p^2 - \tilde{\eta}^2}| \approx h^2 + o(h^2).$$

Then, observing instead that the value of ρ tends to one at the boundaries, it follows that the optimal solution is indeed obtained by equioscillations between the extreme points and the interior point does not play a role. Repeating the analogous calculations of Theorem 2.4, we find that p has the same asymptotic expression as in the previous theorem. We can then conclude that, for $h \to 0$, the two min-max problems with different $\sigma_2(k)$ lead to equivalent optimized parameters. In the nonasymptotic regime, Table 1 shows that the two choices are equivalent for moderate values of $\tilde{\eta}$. For very large values of $\tilde{\eta}$, then (2.9) leads to a more efficient method.

2.2. Zeroth order two sided optimized transmission conditions. Let us consider now the more general case for Robin transmission conditions, with two free parameters p and q such that the operators S_j have eigenvalues

$$\sigma_1(k) = \nu_2 p, \quad \sigma_2(k) = \nu_1 \sqrt{q^2 + \tilde{\eta}^2}.$$

We remark that, according to this choice, $\sigma_1(k)$ is exact for the frequency $k = p$ while $\sigma_2(k)$ is exact for frequency $k = q$. Therefore from (2.6) we deduce the method converges in two iterations for two frequencies. Again letting $\lambda = \frac{\nu_1}{\nu_2}$, we get

(2.15)
$$\min_{p,q} \max_{k_{\min} \le k \le k_{\max}} |\rho(k,p,q)| = \min_{p,q} \max_{k_{\min} \le k \le k_{\max}} \left| \frac{(k-p)(\sqrt{k^2+\tilde{\eta}^2} - \sqrt{q^2+\tilde{\eta}^2})}{(k+\lambda\sqrt{q^2+\tilde{\eta}^2})(\sqrt{k^2+\tilde{\eta}^2} + \frac{p}{\lambda})} \right|.$$

Following the same philosophy of the previous section, we start restricting the range in which we need to search for the parameters p and q. Then we focus on the maxima with respect to k, and finally we analyze how these maxima behave with respect to p and q.

LEMMA 2.7 (restriction for the interval of p, q). *If the couple (p^*, q^*) is a solution to the min-max problem* (2.15)*, then we have that both p^* and q^* belong to the interval $[k_{\min}, k_{\max}]$.*

Proof. For $p > 0$, we observe that $|\rho(k,p,q|) < |\rho(k,-p,q)|$ and q is always squared so we can restrict both parameters to be positive without loss of generality. Next, we consider the partial derivatives of $|\rho|$ with respect to p and q:

$$\text{sign}\left(\frac{\partial|\rho|}{\partial p}\right) = -\text{sign}(k-p), \quad \text{sign}\left(\frac{\partial|\rho|}{\partial q}\right) = -\text{sign}(k-q). \tag{2.16}$$

Repeating the same argument of Lemma 2.1, we conclude that we are not at the optimum unless both p and q belong to $[k_{\min}, k_{\max}]$. ∎

Next, we analyze the behavior of $|\rho(k,p,q)|$ with respect to the variable k, trying to identify the local maxima.

LEMMA 2.8 (local maxima in k). *For $p, q \in [k_{\min}, k_{\max}]$,*

$$\max_{k_{\min} \le k \le k_{\max}} |\rho(k,p,q)| = \max\{|\rho(k_{\min},p,q)|, |\rho(\hat{k},p,q)|, |\rho(k_{\max},p,q)|\},$$

where $\hat{k}$ is an interior maximum always between $[\min(p,q), \max(p,q)]$.

Proof. We first observe that $|\rho(k,p,q)|$ has two zeros, one at $k = p$ and the other at $k = q$. Next, we consider the derivative of $\rho(k,p,q)$ with respect to k and assuming that $p \neq q$[1] we get

$$\begin{aligned}\frac{\partial\rho(k,p,q)}{\partial k} &= \frac{(\sqrt{k^2+\tilde{\eta}^2} - \sqrt{q^2+\tilde{\eta}^2})(\sqrt{k^2+\tilde{\eta}^2})(\sqrt{k^2+\tilde{\eta}^2} + \frac{p}{\lambda})(\lambda\sqrt{q^2+\tilde{\eta}^2} + p)}{D(k,p)} \\ &+ \frac{(k-p)(k+\lambda\sqrt{q^2+\tilde{\eta}^2})k(\frac{p}{\lambda} + \sqrt{q^2+\tilde{\eta}^2})}{D(k,p)}.\end{aligned} \tag{2.17}$$

The denominator $D(k,p)$ is always positive. Now we consider the two cases in which $k < \min(p,q)$ and $k > \max(p,q)$: in both we have that $\rho(k,p,q) > 0$, and analyzing

[1] If $p = q$, we are considering the optimization problem discussed in the previous paragraph.

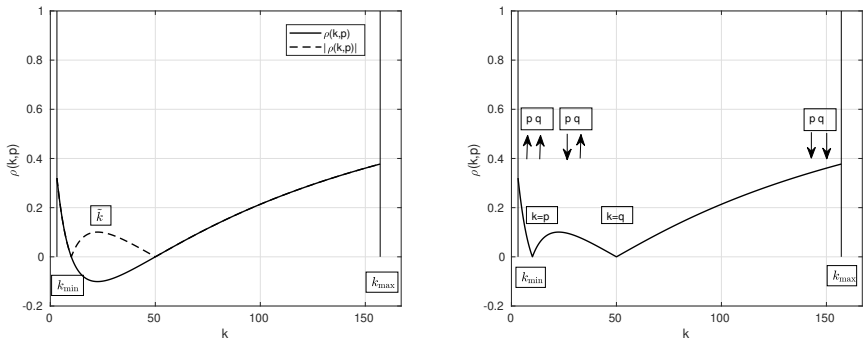

FIG. 3. *The left panel shows an example of the convergence factor with its three local maxima localized at $k = k_{\min}$, $k = k_{\max}$, and $k = \tilde{k}$. On the right we summarize how these local maxima behave as function of p and q.*

(2.17) we conclude that for $k < \min(p,q)$, $\frac{\partial \rho(k,p)}{\partial k} < 0$ and for $k > \max(p,q)$, $\frac{\partial \rho}{\partial k} > 0$. Hence by continuity of $\partial_k \rho(k,p)$, there exists at least one $\hat{k}$, which is a local minimum of $\rho(k,p)$ and a local maximum for $|\rho(k,p)|$ (see Figure 3), such that $\partial_k \rho = 0$, and all of them lie in the interval $[\min(p,q), \max(p,q)]$ for p and q fixed. Now we prove that the interior maximum is unique. Indeed the interior maxima for $|\rho(k,p,q)|$ are given by the roots of $\partial_k \rho(k,p) = 0$ which corresponds to

$$\frac{\sqrt{q^2+\tilde{\eta}^2} - \sqrt{\tilde{\eta}^2+k^2}}{k + \lambda\sqrt{\tilde{\eta}^2+q^2}} = \frac{(k-p)\,k}{\left(\lambda\sqrt{k^2+\tilde{\eta}^2}+p\right)\sqrt{k^2+\tilde{\eta}^2}}. \tag{2.18}$$

First, we suppose that $p < k < q$. Then, we have that the left-hand side of (2.18) is positive in $k = p$, it is strictly decreasing in k, and it reaches zero at $k = q$. The right-hand side of (2.18) instead starts from zero and it is strictly increasing. We conclude that there is a unique point $\hat{k}$ such that the two sides are equal and hence a unique interior maximum $\hat{k}$ for $|\rho(k,p,q)|$. If $q < k < p$, changing the sign of (2.18) and diving by $k/\sqrt{k^2+\tilde{\eta}^2}$, the right-hand side is strictly decreasing while the left-hand side, computing the derivative, is strictly increasing and hence the same conclusion holds.

We may conclude that the function assumes its maximum either at the interior point $\hat{k}$, or at the boundaries of the interval, i.e., $k_{\min}$, $k_{\max}$. ∎

In the next lemma we prove that the end points $k_{\min}$ and $k_{\max}$ satisfy an equioscillation property as in the previous case of a single parameter p.

LEMMA 2.9 (equioscillation at the end points). *The optimized convergence factor $|\rho(k,p,q)|$ must satisfy equioscillation at the end points, i.e.,*

$$|\rho(k_{\min}, p^*, q^*)| = |\rho(k_{\max}, p^*, q^*)|.$$

Proof. We study how $|\rho(k_{\min},p,q)|$, $|\rho(\tilde{k},p,q)|$, and $|\rho(k_{\max},p,q)|$ behave as p,q vary, and we show that if we do not have equioscillation at the boundary points, we can always improve the convergence factor until equioscillation is reached. Taking into account (2.16), we have for every $p,q \in [k_{\min}, k_{\max}]$

$$\frac{\partial|\rho(k_{\min},p,q)|}{\partial p} > 0, \quad \frac{\partial|\rho(k_{\min},p,q)|}{\partial q} > 0,$$

$$\frac{\partial|\rho(k_{\max},p,q)|}{\partial p}<0,\quad \frac{\partial|\rho(k_{\max},p,q)|}{\partial q}<0.$$

In other words, increasing independently p,q increases $|\rho(k_{\min},p,q)|$ and decreases $|\rho(k_{\max},p,q)|$. We now compute the total derivative of $|\rho(\tilde{k},p,q)|$ with respect to p and q, which since we have $\partial_k|\rho(\tilde{k},p,q)|=0$, corresponds to the partial derivative with respect to the two arguments. One then finds that the sign of $\frac{\partial|\rho(\tilde{k},p,q)|}{\partial p}$ and $\frac{\partial|\rho(\tilde{k},p,q)|}{\partial q}$ depends on the position of $\tilde{k}$ with respect to p and q. Indeed, it holds that

$$\operatorname{sign}\left(\frac{\partial|\rho(\tilde{k},p,q)|}{\partial p}\right)=\operatorname{sign}(p-\tilde{k}),\quad \operatorname{sign}\left(\frac{\partial|\rho(\tilde{k},p,q)|}{\partial q}\right)=\operatorname{sign}(q-\tilde{k}).$$

The right panel of Figure 3 summarizes the dependence of the local maxima with respect to p and q. Let us suppose that $p<q$, q fixed, and $|\rho(k_{\min},p,q)|<|\rho(k_{\max},p,q)|$. The other cases are treated similarly. We do not make any assumptions on the value of $|\rho(\tilde{k},p,q)|$. Now if we increase p, we decrease $\max\{|\rho(k_{\min},p,q)|,|\rho(\hat{k},p,q)|,|\rho(k_{\max},p,q)|\}$ as long as $|\rho(k_{\min},p,q)|\le|\rho(k_{\max},p,q)|$ and $p\le q$. If $|\rho(k_{\min},p,q)|=|\rho(k_{\max},p,q)|$ for a certain $p<q$, then we obtain the desired result since we have improved uniformly the convergence factor. Suppose instead that when $p=q$, and therefore $|\rho(\tilde{k},p,q)|=0$, we still have $|\rho(k_{\min},p,q)|<|\rho(k_{\max},p,q)|$. Thus the convergence factor is equal to $|\rho(k_{\max},p,q)|$. We now set up a process which improves $\max_{[k_{\min},k_{\max}]}|\rho(k,p,q)|$ until we get equioscillation at the boundary points. As long as $|\rho(k_{\min},p,q)|<|\rho(k_{\max},p,q)|$, we increase $p>q$ until $|\rho(\tilde{k},p,q)|\le|\rho(k_{\max},p,q)|$. When we reach $|\rho(\tilde{k},p,q)|=|\rho(k_{\max},p,q)|$, we then increase q until $q=p$. If while increasing q we still have $|\rho(k_{\min},p,q)|<|\rho(k_{\max},p,q)|$, then we repeat the process. Continuing this process, we must reach equioscillation at some point by continuity since when p approaches $k_{\max}$, we must have $|\rho(k_{\min},k_{\max},q)|>|\rho(k_{\max},k_{\max},q)|=0$. At the same time we improved surely the convergence factor since, in spite of the initial value of $|\rho(\tilde{k},p,q)|$, we have that $\max_{[k_{\min},k_{\max}]}|\rho(k,p,q)|\le|\rho(k_{\max},p,q)|$ which is decreasing along the process. ∎

We now have enough tools and insights to prove the main results of this section.

THEOREM 2.10. *There are two pairs of parameters (p_1^*,q_1^*) and (p_2^*,q_2^*) such that we obtain equioscillation between all three local maxima,*

$$|\rho(k_{\min},p_j^*,q_j^*)|=|\rho(k_{\max},p_j^*,q_j^*)|=|\rho(\hat{k},p_j^*,q_j^*)|,\quad j=1,2. \tag{2.19}$$

The optimal pair of parameters is the one which realizes the

$$\min_{(p_j^*,q_j^*),j=1,2}|\rho(k_{\min},p_j^*,q_j^*)|. \tag{2.20}$$

Proof. Let us define $F_1(p,q):=\rho(k_{\min},p,q)$ and $F_2(p,q):=\rho(k_{\max},p,q)$. Due to Lemma 2.9, we know that there exist values (p,q) such that $F:=|F_1(p,q)|-|F_2(p,q)|=0$. We can thus express one parameter, for example q, as a function of the other one, i.e., $q=q(p)$. Although the expression is too complicated to be used for analytical computations, we are able to infer about the structure of $q(p)$. First, we can state that $q(p=k_{\min})=k_{\max}$ since $|F_1(k_{\min},q(k_{\min}))|=0$ implies that $|F_2(k_{\min},q(k_{\min})|=0$ but then the only choice possible is $q(k_{\min})=k_{\max}$. Similarly, we have $q(k_{\max})=k_{\min}$. We next use implicit differentiation to infer about the behavior of q with respect to p.

Following classical arguments, we have that, since $F(p, q(p)) = 0$,

$$0 = \frac{dF(p,q(p))}{dp} = \frac{dF_1(p,q(p)) - dF_2(p,q(p))}{dp} = \frac{\partial F_1 - \partial F_2}{\partial p} + \frac{\partial F_1 - \partial F_2}{\partial q} q'(p),$$

and therefore,

$$q'(p) = \frac{\frac{\partial F_2}{\partial p} - \frac{\partial F_1}{\partial p}}{\frac{\partial F_1}{\partial q} - \frac{\partial F_2}{\partial q}}. \tag{2.21}$$

Analyzing carefully the sign of each term, we conclude that $q'(p) < 0 \; \forall p \in (k_{\min}, k_{\max})$. Therefore, we state that $q(p)$ is a strictly decreasing function which starts from $q(p = k_{\min}) = k_{\max}$ and reaches its minimum at $q(k_{\max}) = k_{\min}$.

Now we have only one free parameter p, since q is constrained to vary such that the equioscillation between the end points is achieved, thus we look for values of p such that we obtain equioscillation between $k_{\min}$ and the interior maximum $\hat{k}$.

Let us first study how $\tilde{F}(p, q) := \rho(\hat{k}, p, q(p))$ behaves while p varies. As long as $p \le \hat{k} \le q(p)$, we have

$$\operatorname{sign}\left(\frac{\partial |\tilde{F}(p,q(p))|}{\partial p}\right) = \operatorname{sign}\left(\sqrt{q(p)^2 + \tilde{\eta}^2} - \sqrt{\hat{k}^2 + \tilde{\eta}^2}\right) \cdot \operatorname{sign}(\tilde{F}(p, q(p)) < 0,$$

$$\operatorname{sign}\left(\frac{\partial |\tilde{F}(p,q(p))|}{\partial q}\right) = \operatorname{sign}(p - \hat{k}) \cdot \operatorname{sign}(\tilde{F}(p, q(p)) > 0.$$

Then, keeping in mind the $q'(p) < 0$, $\tilde{F}(p, q(p))$ is strictly decreasing for all of the values of p such that $p < \hat{k} < q(p)$,

$$\frac{d|\tilde{F}(p,q(p))|}{dp} = \frac{\partial |\tilde{F}(p,q(p))|}{\partial p} + \frac{\partial |\tilde{F}(p,q(p))|}{\partial q} \cdot q'(p) < 0.$$

Similarly, it is straightforward to verify that for $q(p) < \hat{k} < p$,

$$\frac{d|\tilde{F}(p,q(p))|}{dp} = \frac{\partial |\tilde{F}(p,q(p))|}{\partial p} + \frac{\partial |\tilde{F}(p,q(p))|}{\partial q} \cdot q'(p) > 0.$$

Moreover, we have that for $p = \hat{k} = q(p)$, $|\tilde{F}(p, q(p))| = 0$ and $\frac{d|\tilde{F}(p,q(p))|}{dp} = 0$.

Focusing next on $|F_1(p, q(p))|$ we can state that, neglecting the $\operatorname{sign}(F_1(p, q(p)))$, because it is always positive or zero, the derivatives at the left and right boundary extrema are equal to

$$\begin{aligned}\frac{d|F_1(k_{\min}, k_{\max})|}{dp} &= \frac{\partial |F_1(k_{\min}, k_{\max})|}{\partial p} + \frac{\partial |F_1(k_{\min}, k_{\max})|}{\partial q} q'(p) \\ &= \frac{\partial |F_1(k_{\min}, k_{\max})|}{\partial p} > 0\end{aligned}$$

and

$$\begin{aligned}\frac{d|F_1(k_{\max}, k_{\min})|}{dp} &= \frac{\partial |F_1(k_{\max}, k_{\min})|}{\partial p} + \frac{\partial |F_1(k_{\max}, k_{\min})|}{\partial q} q'(p) \\ &= \frac{\partial |F_1(k_{\max}, k_{\min})|}{\partial p} < 0.\end{aligned}$$

So for values of p in a right neighborhood of $p = k_{\min}$, $|F_1(p, q(p))|$ increases, while for values of p in a left neighborhood of $p = k_{\max}$, $|F_1(p, q(p))|$ decreases. Using the monotonicity of $|F(\hat{k}, p, q(p))|$ and the fact that when $\hat{k} = p = q(p)$, $|F(\hat{k}, p, q(p))| = 0$, while $|F(k_{\min}, p, q(p))| > 0$, we conclude that there exists at least one pair (p, q) such that $|F(k_{\min}, p, q(p))| = |F(\hat{k}, p, q(p))|$.

We still have to prove that actually there exist only two couples (p_j, q_j) such that equioscillation is achieved. Indeed, if we imagine that $|F_1(p, q(p))|$ had a certain behavior, for example it oscillates, then we might have more than two pairs. Nevertheless, we show that $|F_1(p, q(p))|$ has a unique local maximum for $p \in [k_{\min}, k_{\max}]$ so that only two equioscillations are allowed among all of the three local maxima: one while $|\tilde{F}(p, q(p))|$ decreases, the other one for increasing $|\tilde{F}(p, q(p))|$.

To do so, we consider $\frac{d|F_1(p,q(p))|}{dp}$ again and substitute (2.21),

$$\frac{d|F_1(p, q(p))|}{dp} = \frac{\frac{\partial F_1}{\partial q} \cdot \frac{\partial F_2}{\partial p} - \frac{\partial F_2}{\partial q} \cdot \frac{\partial F_1}{\partial p}}{\frac{\partial F_1}{\partial q} \cdot \frac{\partial F_2}{\partial q}}.$$

The zeros of the derivative are given by the nonlinear equation

$$\begin{aligned}
&(p - k_{\min})\left(\sqrt{k_{\max}^2 + \tilde{\eta}^2} - \sqrt{k_{\min}^2 + \tilde{\eta}^2}\right) \frac{\sqrt{k_{\min}^2 + \tilde{\eta}^2} + \frac{p}{\lambda}}{\sqrt{k_{\max}^2 + \tilde{\eta}^2} + \frac{p}{\lambda}} \\
&= (k_{\max} - p)\left(\sqrt{q^2 + \tilde{\eta}^2} - \sqrt{k_{\min}^2 + \tilde{\eta}^2}\right) \frac{k_{\min} + \lambda\sqrt{q^2 + \tilde{\eta}^2}}{k_{\max} + \lambda\sqrt{q^2 + \tilde{\eta}^2}}.
\end{aligned}$$

It is sufficient to observe that the left-hand side starts from 0 and it is strictly increasing in p, while the right-hand side starts from a positive value, it decreases with p and it reaches 0 for $p = k_{\max}$. So the equation admits only one solution and, therefore, the local maximum with respect to p of $|F_1(p, q(p))|$ is unique. The solution to the min-max problem (2.15) is the pair of parameters (p^*, q^*) which allows equioscillation among the three local maxima and realizes (2.20). Every other pair of parameter would lead to the increase of at least one of the local maxima and, therefore, of the maximum of $|\rho|$ over k. ∎

In [12], the authors proved a similar result for the Laplace equation with discontinuous coefficients without the presence of the further optimality condition (2.20). Their result was based on the possibility of restricting the interval of interest for the parameters to $p < q$ or $q < p$ according to the value of λ. In the present case this is not possible because of the presence of $\tilde{\eta}^2$, which breaks the symmetry of the convergence factor. Therefore, we cannot discard a priori one of the two possible equioscillations and the further condition (2.20) must be added. Nevertheless, in the asymptotic regime for $h \to 0$ and $k_{\max} \to \infty$, the next result allows us to clearly choose the optimal pair as a function of λ, recovering the property of the results for the simplified situation treated in [12].

THEOREM 2.11. *Let $D := \sqrt{k_{\min}^2 + \tilde{\eta}^2}$. Then if the physical parameters $\tilde{\eta}^2, \nu_1, \nu_2$ are fixed, $k_{\max} = \frac{\pi}{h}$ and h goes to zero, the optimized two-sided Robin parameters are for $\lambda \geq 1$,*

$$\begin{aligned}
&p_1^* \sim \tfrac{\lambda(k_{\min}+D)}{\lambda-1} - \tfrac{2\sqrt{2}(1+\lambda)(\lambda D+k_{\min})\lambda^2\sqrt{\pi(k_{\min}+D)}}{\pi\lambda(\lambda-1)^3} h^{\frac{1}{2}}, \\
&q_1^* \sim \tfrac{\pi(\lambda-1)}{2\lambda} h^{-1} + \tfrac{\sqrt{2}(1+\lambda)^2\sqrt{\pi(k_{\min}+D)}}{2\lambda(\lambda-1)} h^{-\frac{1}{2}}, \\
&\max_{k_{\min} \leq k \leq \pi/h} |\rho(k, p_1^*, q_1^*)| \sim \tfrac{1}{\lambda} - \tfrac{2\sqrt{2}(1+\lambda)\sqrt{(k_{\min}+D)}}{\sqrt{\pi}\lambda(\lambda-1)} h^{\frac{1}{2}},
\end{aligned} \tag{2.22}$$

and for $\lambda < 1$ we have

$$
\begin{aligned}
&p_2^* \sim \tfrac{1}{2}\pi(1-\lambda)h^{-1} + \tfrac{\sqrt{2}(1+\lambda)^2\sqrt{\pi(D+k_{\min})}}{2(1-\lambda)}h^{-\frac{1}{2}},\\
&q_2^* \sim \sqrt{\left(\tfrac{D+k_{\min}}{1-\lambda}\right)^2 - \tilde{\eta}^2} - \tfrac{2\sqrt{2}(D+k_{\min})^2(\lambda+1)(\lambda D+k_{\min})}{(\lambda-1)^4\sqrt{\pi(D+k_{\min})}\sqrt{\frac{D+k_{\min}}{1-\lambda}-\tilde{\eta}^2}}h^{\frac{1}{2}},\\
&\max_{k_{\min}\le k\le \pi/h}|\rho(k,p_2^*,q_2^*)| \sim \lambda - \tfrac{2\sqrt{2}\lambda(1+\lambda)\sqrt{(k_{\min}+D)}}{\sqrt{\pi}(1-\lambda)}h^{\frac{1}{2}}.
\end{aligned}
\tag{2.23}
$$

Proof. Guided by numerical experiments, for $\lambda \ge 1$ we make the ansatz $p \sim C_p + Ah^{\frac{1}{2}}$, $q \sim Qh^{-1} + Bh^{-\frac{1}{2}}$, and $\hat{k} = C_k h^{-\frac{1}{2}}$. First, considering $\partial_k \rho(\hat{k}, p, q) = 0$, we find setting to zero the first nonzero term $C_k = \sqrt{C_p \cdot Q}$. Inserting this into (2.19) and comparing the two leading terms, we get the result. Similarly, for $\lambda < 1$, we make the ansatz $p \sim C_p h^{-1} + Ah^{-\frac{1}{2}}$, $q \sim Q + Bh^{\frac{1}{2}}$, and $\hat{k} = C_k h^{-\frac{1}{2}}$, and we get $C_k = \sqrt{C_p\sqrt{Q^2+\tilde{\eta}^2}}$. Substituting and matching the leading order terms we obtain the result. ∎

If we set $\tilde{\eta}^2 = 0$, then $D = k_{\min}$ and we recover the results of [12]. Note that in contrast to the one sided case, the convergence factor does not deteriorate to 1 as $h \to 0$, but it is bounded either by $\frac{1}{\lambda}$ if $\lambda \ge 1$ or by λ if $\lambda < 1$, so we obtain a nonoverlapping optimized Schwarz method that converges independently of the mesh size h. We emphasize that the heterogeneity makes the method faster instead of presenting a difficulty. A heuristic explanation is that the heterogeneity tends to decouple the problems, making them less dependent one from the other. In contrast with other domain decomposition methods, optimized Schwarz methods can be tuned according to the physics and, therefore, they can benefit from this decoupling.

3. Advection reaction diffusion-reaction diffusion coupling. In this section, we consider again a domain Ω divided into two subdomains, Ω_1, Ω_2 according to the description at the beginning of section 2. In Ω_1 we have a reaction diffusion equation, while in Ω_2 we have an advection reaction diffusion equation. We allow the reaction and diffusion coefficients to be different among the subdomains. The optimized Schwarz method reads

$$
\begin{aligned}
(\eta_1^2 - \nu_1\Delta)u_1^n &= f \quad \text{in} \quad \Omega_1,\\
(\nu_1\partial_x + S_1)(u_1^n)(0,\cdot) &= (\nu_2\partial_x - \mathbf{a}\cdot(1,0)^\top + S_1)(u_2^{n-1})(0,\cdot),\\
(\eta_2^2 + \mathbf{a}\cdot\nabla - \nu_2\Delta)u_2^n &= f \quad \text{in} \quad \Omega_2,\\
(\nu_2\partial_x - \mathbf{a}\cdot(1,0)^\top - S_2)(u_2^n)(0,\cdot) &= (\nu_1\partial_x - S_2)(u_1^{n-1})(0,\cdot),
\end{aligned}
\tag{3.1}
$$

where $\mathbf{a} = (a_1, a_2)^\top$. The additional term in the transmission conditions arises from the conservation of the flux in divergence form; see Chapter 6 in [31]. We first suppose $a_2 = 0$. Then, we can solve the error equations in the subdomains through separation of variables and we obtain $e_i^n = \sum_{k\in\mathcal{V}} \hat{e}_i^n \sin(ky)$, $i = 1, 2$, where

$$
\hat{e}_1^n(k,x) = A^n(k)e^{\sqrt{\frac{\eta_1^2}{\nu_1}+k^2}x}, \qquad \hat{e}_2^n(k,x) = B^n(k)e^{\lambda_-(k)x},
$$

and $\lambda_-(k) := \frac{a_1-\sqrt{a_1^2+4\nu_2^2k^2+4\nu_2\eta_2^2}}{2\nu_2}$. Inserting e_1, e_2 into the transmission conditions we get

$$\nu_1\sqrt{\frac{\eta_1^2}{\nu_1}+k^2}A^n(k)+\sigma_1(k)A^n(k)=\nu_2\lambda_-(k)B^{n-1}(k)-a_1B^{n-1}(k)+\sigma_1(k)B^{n-1}(k),$$

$$\nu_2\lambda_-(k)B^n(k)-a_1B^n(k)-\sigma_2(k)B^n(k)=\nu_1\sqrt{\frac{\eta_1^2}{\nu_1}+k^2}A^{n-1}(k)-\sigma_2(k)A^{n-1}(k).$$

The convergence factor is given by

$$\rho(k,\sigma_1,\sigma_2)=\frac{\nu_2\lambda_-(k)-a_1+\sigma_1(k)}{\nu_1\sqrt{\tilde{\eta}_1^2+k^2}+\sigma_1(k)}\frac{\nu_1\sqrt{\tilde{\eta}_1^2+k^2}-\sigma_2(k)}{\nu_2\lambda_-(k)-a_1-\sigma_2(k)},$$

where $\tilde{\eta}_1^2=\frac{\eta_1^2}{\nu_1}$. We rewrite $\lambda_-(k)$ as $\lambda_-(k)=\frac{a_1}{2\nu_2}-\sqrt{k^2+\delta^2}$ with $\delta^2=\frac{a_1^2}{4\nu_2^2}+\frac{\eta_2^2}{\nu_2}$. Using the dependence on k, the convergence factor becomes

$$\rho(k,\sigma_1,\sigma_2)=\frac{\nu_2\sqrt{k^2+\delta^2}+\frac{a_1}{2}-\sigma_1(k)}{\nu_1\sqrt{\tilde{\eta}_1^2+k^2}+\sigma_1(k)}\frac{\nu_1\sqrt{\tilde{\eta}_1^2+k^2}-\sigma_2(k)}{\nu_2\sqrt{k^2+\delta^2}+\frac{a_1}{2}+\sigma_2(k)}.$$

We can define the two optimal operators S_j^{opt} associated to the eigenvalues $\sigma_1^{\text{opt}}(k):=\nu_2\sqrt{k^2+\delta^2}+\frac{a_1}{2}$ and $\sigma_2^{\text{opt}}(k):=\nu_1\sqrt{k^2+\tilde{\eta}_1^2}$ which lead to convergence in just two iterations.

3.1. Zeroth order single sided optimized transmission conditions. Following the strategy of the previous section, we choose $\sigma_1(k),\sigma_2(k)$ so that they coincide with the optimal choice for the frequency $k=p$, i.e., $\sigma_1(k)=\nu_2\sqrt{p^2+\delta^2}+\frac{a_1}{2}$ and $\sigma_2(k)=\nu_1\sqrt{p^2+\tilde{\eta}_1^2}$. Defining $\lambda:=\frac{\nu_1}{\nu_2}$, the convergence factor then becomes

$$\rho(k,p)=\frac{\sqrt{k^2+\tilde{\eta}_1^2}-\sqrt{p^2+\tilde{\eta}_1^2}}{\frac{1}{\lambda}\left(\sqrt{k^2+\delta^2}+\frac{a_1}{2\nu_2}\right)+\sqrt{p^2+\tilde{\eta}_1^2}}\cdot\frac{\sqrt{k^2+\delta^2}-\sqrt{p^2+\delta^2}}{\lambda\sqrt{k^2+\tilde{\eta}_1^2}+\left(\sqrt{p^2+\delta^2}+\frac{a_1}{2\nu_2}\right)}. \tag{3.2}$$

THEOREM 3.1. *The unique optimized Robin parameter p^* solving the min-max problem*

$$\min_{p\in\mathbb{R}}\max_{k_{\min}\le k\le k_{\max}}|\rho(k,p)|, \tag{3.3}$$

is given by the unique root of the nonlinear equation

$$|\rho(p^*,k_{\min})|=|\rho(p^*,k_{\max})|.$$

Proof. The proof is very similar to the proof of Theorem 2.3; therefore, we just sketch the main steps. We start observing that $\rho(k,p)$ has only one zero located at $k=p$ and $\rho(k,p)>0\ \forall k,p$. Thus we may neglect the absolute value. Analyzing the derivative with respect to p, we find that

$$\operatorname{sign}\left(\frac{\partial\rho(k,p)}{\partial p}\right)=-\operatorname{sign}(k-p).$$

This implies that $\frac{\partial \rho(k,p)}{\partial p} > 0$ if $k < p$ and $\frac{\partial \rho(k,p)}{\partial p} < 0$ if $k > p$. We conclude that p must lie in the interval $[k_{\min}, k_{\max}]$. Similarly, the derivative with respect to k satisfies $\frac{\partial \rho(k,p)}{\partial k} < 0$ if $k < p$ and $\frac{\partial \rho(k,p)}{\partial k} > 0$ if $k > p$. Hence, the local maxima with respect to k are located at the boundary points $k = k_{\min}$ and $k = k_{\max}$. Repeating the final argument of Theorem 2.3 we get the result. ∎

Since a closed form formula is again not available, we now show asymptotic results for the optimal parameter p^* and observe the behavior of the method when taking finer and finer meshes.

THEOREM 3.2. *If the physical parameters are fixed, $k_{\max}=\frac{\pi}{h}$, and h is small enough, then the optimized Robin parameter p^* satisfies*

$$p^* \sim C_a \cdot h^{-\frac{1}{2}},\ C_a = \frac{\sqrt{\nu_2\ (\lambda+1)\,\pi\ \left(2\sqrt{k_{\min}^2+\tilde{\eta}_1^2}\lambda\,\nu_2 + 2\sqrt{k_{\min}^2+\delta^2}\nu_2 - a_1\right)}}{\sqrt{2}\nu_2\ (\lambda+1)}.$$

Furthermore, the asymptotic convergence factor is

$$\max_{k_{\min}\le k\le \pi/h} |\rho(k,p^*)| \sim 1 - h^{\frac{1}{2}}\left(\frac{C_a\ (\lambda+1)^2}{\lambda\,\pi}\right).$$

Proof. We insert the ansatz $p = C_a \cdot h^{-\alpha}$ into (3.3). Expanding for small h, we get that

$$\rho(p, k_{\min}) \sim 1 - h^{\alpha}\left(\frac{C_a\ (\lambda+1)^2}{\lambda\,\pi}\right).$$

On the other hand,

$$\rho(p, k_{\max}) \sim 1 + h^{-\alpha+1}\left(\frac{1}{2}\,\frac{(\lambda+1)\left(-2\sqrt{k_{\min}^2+\tilde{\eta}_1^2}\lambda\,\nu_2 - 2\sqrt{k_{\min}^2\delta^2}\nu_2 + a_1\right)}{C_a\,\nu_2\,\lambda}\right).$$

Comparing the first two terms we get the result. ∎

3.2. Zeroth order two sided optimized transmission conditions. In this paragraph we generalize the previous transmission conditions, introducing another degree of freedom q. The operators S_j are such that their eigenvalues are

$$\sigma_1(k) = \nu_2\sqrt{q^2+\delta^2} + \frac{a_1}{2}, \qquad \sigma_2(k) = \nu_1\sqrt{p^2+\tilde{\eta}_1^2},$$

and the convergence factor becomes

$$\rho(k,p) = \frac{\sqrt{k^2+\tilde{\eta}_1^2} - \sqrt{p^2+\tilde{\eta}_1^2}}{\frac{1}{\lambda}\left(\sqrt{k^2+\delta^2}+\frac{a_1}{2\nu_2}\right) + \sqrt{p^2+\tilde{\eta}_1^2}} \cdot \frac{\sqrt{k^2+\delta^2} - \sqrt{q^2+\delta^2}}{\lambda\sqrt{k^2+\tilde{\eta}_1^2} + \left(\sqrt{q^2+\delta^2}+\frac{a_1}{2\nu_2}\right)}.$$

In order to prove a similar result as in Theorem 2.10, we suppose that $\tilde{\eta}_1 = 0$, i.e., only diffusion is present in Ω_1, and $a_1 > 0$, i.e., the advection flux is pointing into the subdomain Ω_2.

THEOREM 3.3. *There are two pairs of parameters (p_1^*, q_1^*) and (p_2^*, q_2^*) such that we obtain equioscillation between all of the three local maxima located at the boundary extrema $k_{\min}, k_{\max}$ and at the interior point $\hat{k}$,*

$$|\rho(k_{\min}, p_j^*, q_j^*)| = |\rho(k_{\max}, p_j^*, q_j^*)| = |\rho(\hat{k}, p_j^*, q_j^*)|, \quad j = 1, 2.$$

The optimal pair of parameters is the one which realizes the

$$\min_{(p_j^*,q_j^*),j=1,2} |\rho(k_{\min}, p_j^*, q_j^*)|.$$

Proof. Similarly to the proof of Theorem 2.10, we observe that the function admits two zeros, one located at $k = p$, the other at $k = q$ due to the choice of the transmission operators. Computing the derivatives with respect to p and q we get

$$\operatorname{sign}\left(\frac{\partial|\rho|}{\partial p}\right) = -\operatorname{sign}(\rho)\cdot\operatorname{sign}(k-q) = -\operatorname{sign}(k-p),$$
$$\operatorname{sign}\left(\frac{\partial|\rho|}{\partial q}\right) = -\operatorname{sign}(\rho)\cdot\operatorname{sign}(k-p) = -\operatorname{sign}(k-q).$$

We conclude that, at the optimum, both p and q lie in $[k_{\min}, k_{\max}]$, i.e., the function at the optimum has two zeros in the interval. Now we study the behavior with respect to k. Computing the derivative with respect to k, we find that the potential local maxima are given by the roots of

$$\frac{\sqrt{\delta^2+k^2}-\sqrt{\delta^2+q^2}}{k(\lambda k+\sqrt{q^2+\delta^2}+\frac{a_1}{2\nu_2})} = \frac{p-k}{\sqrt{k^2+\delta^2}\left(p\lambda+\sqrt{k^2+\delta^2}+\frac{a_1}{2\nu_2}\right)}.$$

With some algebraic manipulations, we find that a sufficient condition such that $\frac{p-k}{(p\lambda+\sqrt{k^2+\delta^2}+a_1/(2\nu_2))}$ has a monotonic behavior with respect to k is that $a_1 > 0$. Then under this hypothesis we may repeat the arguments in the proof of Theorem 2.10. Letting p, q in $[k_{\min}, k_{\max}]$, we have that the local maxima of the function are located at $k_{\min}, k_{\max}, \hat{k}$. Moreover, we have

$$\begin{aligned}
&\frac{\partial|\rho|}{\partial p}|_{k=k_{\min}} > 0, && \frac{\partial|\rho|}{\partial q}|_{k=k_{\min}} > 0,\\
&\frac{\partial|\rho|}{\partial p}|_{k=k_{\max}} < 0, && \frac{\partial|\rho|}{\partial q}|_{k=k_{\max}} < 0,\\
&\frac{\partial|\rho|}{\partial p}|_{k=\tilde{k}} < 0, && \frac{\partial|\rho|}{\partial q}|_{k=\tilde{k}} > 0.
\end{aligned} \tag{3.4}$$

We can thus repeat the same arguments as in the proof of Theorem 2.10 since all steps are now exclusively based on the sign of the partial derivatives with respect to the parameters (see (3.4)), and the result follows. ∎

THEOREM 3.4. *Let $D := \sqrt{k_{\min}^2+\delta^2}$. If the physical parameters $\tilde{\eta}_2^2, \nu_1, \nu_2, a_1$ are fixed, $k_{\max} = \frac{\pi}{h}$ and h goes to zero, the optimized two-sided Robin parameters are for $\lambda \geq 1$,*

$$p_1^* \sim P_1 h^{-1} + E_1 h^{-\frac{1}{2}}, \quad q_1^* \sim Q_1 - F_1 h^{\frac{1}{2}}, \quad \max_{k_{\min}\leq k\leq \frac{\pi}{h}} |\rho(k, p_1^*, q_1^*)| \sim \lambda - \frac{E_1\pi(\lambda+1)}{(P_1\lambda+\pi)^2} h^{\frac{1}{2}},$$

with

$$P_1 := \frac{\pi(\lambda-1)}{2\lambda}, \quad Q_1 := \sqrt{\frac{D + k_{\min} + \frac{a_1}{2\nu_2\lambda}}{1-\frac{1}{\lambda}} - \delta^2},$$
$$E_1 := \frac{(2(P_1\sqrt{\delta^2+Q_1^2}+C_h^2)(\lambda+1)\nu_2 + P_1 a_1)(\lambda P_1+\pi)^2}{2\lambda^2 P_1\nu_2 C_h \pi(\lambda+1)},$$
$$F_1 := \frac{(2(P_1\sqrt{\delta^2+Q_1^2}+C_h^2)(\lambda+1)\nu_2 + P_1 a_1)(2\nu_2(\lambda k_{\min}+\sqrt{\delta^2+Q_1^2})+a_1)^2\sqrt{\delta^2+Q_1^2}}{4\lambda^2 P_1\nu_2^2 C_h Q_1(2\nu_2(\lambda k_{\min}+D)+a_1)},$$
$$C_h := \frac{\sqrt{P_1(2\sqrt{\delta^2+Q_1^2}\nu_2(\lambda+1)+a_1)}}{\sqrt{2\nu_2(\lambda+1)}},$$

and for $\lambda < 1$,

$$p_2^* \sim P_2 - E_2 h^{\frac{1}{2}}, \quad q_2^* \sim Q_2 h^{-1} + F_2 h^{-\frac{1}{2}}, \quad \max_{k_{\min}\le k\le \frac{\pi}{h}} |\rho(k,p_2^*,q_2^*)| \sim \lambda - \frac{F_2\lambda\pi(1+\lambda)}{(\lambda\pi+Q_2)^2} h^{\frac{1}{2}}$$

with

$$P_2 := \frac{D + k_{\min} + \frac{a_1}{2\nu_2}}{1-\lambda}, \quad Q_2 := \frac{\pi(\lambda-1)}{2},$$
$$E_2 := \frac{((\lambda+1)(D_h^2+P_2Q_2)\nu_2 + \frac{a_1Q_2}{2})(2\nu_2(\lambda P_2+D)+a_1)^2}{2\nu_2^2 D_h Q_2(2k_{\min}\lambda\nu_2 + 2\nu_2 D + a_1)},$$
$$F_2 := \frac{\sqrt{\lambda+1}\sqrt{(D+k_{\min})(\lambda+1)+\frac{a_1}{2\nu_2}}\sqrt{\pi}(3\lambda-1)^2}{\sqrt{2}(1-\lambda^2)},$$
$$D_h := \frac{\sqrt{Q_2(2P_2\nu_2(\lambda+1)+a_1)}}{\sqrt{2\nu_2(\lambda+1)}}.$$

Proof. The proof follows the same steps as in the proof of Theorem 2.11. ∎

3.3. Advection tangential to the interface. In the previous subsection we restricted our study to the case of advection normal to the interface. Here we consider the other relevant physical case, namely advection tangential to the interface, so that $a_1 = 0$ and $a_2 \neq 0$ in (3.1). For homogeneous problems, this case has been studied through Fourier transform in unbounded domains; see [7]. However, it has recently been observed in [18], that for homogeneous problems with tangential advection this procedure does not yield efficient optimized parameters. The reason behind this failure lies in the separation of variables technique which applied to the error equation,

$$\begin{aligned}
(\eta_1^2 - \nu_1\Delta)e_1^n &= 0 \quad \text{in} \quad \Omega_1,\\
(\nu_1\partial_x + S_1)(e_1^n)(0,\cdot) &= (\nu_2\partial_x + S_1)(e_2^{n-1})(0,\cdot),\\
(\eta_2^2 + a_2\partial_y - \nu_2\Delta)e_2^n &= 0 \quad \text{in} \quad \Omega_2,\\
(\nu_2\partial_x - S_2)(e_2^n)(0,\cdot) &= (\nu_1\partial_x - S_2)(e_1^{n-1})(0,\cdot)
\end{aligned} \tag{3.5}$$

leads to

$$e_1^n = \sum_{k\in\mathcal{V}} \hat{e}_1^n(0,k) e^{\lambda_1(k)x}\sin(ky) \quad \text{and} \quad e_2^n = \sum_{k\in\mathcal{V}} \hat{e}_2^n(0,k) e^{-\lambda_2(k)x} e^{\frac{a_2 y}{2\nu_2}}\sin(ky), \tag{3.6}$$

where $\lambda_1(k) = \sqrt{k^2+\tilde{\eta_1}}$, $\lambda_2(k) = \frac{\sqrt{4\nu_2^2k^2+4\nu_2^2\tilde{\eta_2}^2+a_2^2}}{2\nu_2}$ with $\tilde{\eta}_j^2 := \frac{\eta_j^2}{\nu_j}$. Since the functions $\psi_k(y) := \sin(ky)$ and $\phi_k(y) := e^{\frac{a_2 y}{2\nu_2}}\sin(ky)$ are not orthogonal, it is not possible to obtain a recurrence relation which expresses $\hat{e}_j^n(0,k)$ only as a function of $\hat{e}_j^{n-2}(0,k)$

for each k and $j = 1, 2$. Nevertheless, we propose here a more general approach. First, let us define two scalar products, the classical L^2 scalar product $\langle f, g\rangle = \frac{2}{L}\int_\Gamma fg dy$ and the weighted scalar product $\langle f, g\rangle_{\rm w} = \frac{2}{L}\int_\Gamma fge^{-\frac{a_2 y}{\nu_2}} dy$. It follows that $\langle \psi_k, \psi_j\rangle = \delta_{k,j}$ and $\langle \phi_k, \phi_j\rangle_{\rm w} = \delta_{k,j}$. Setting $S_1 := \nu_2\lambda_2(p)$ and $S_2 := \nu_1\lambda_1(q)$ for $p, q \in \mathbb{R}$ and inserting the expansions (3.6) into the boundary conditions of (3.5), we obtain

(3.7)
$$\sum_{i=1}^{+\infty} \hat{e}_1^n(0,i)(\nu_1\lambda_1(i) + \nu_2\lambda_2(p))\psi_i(y) = \sum_{l=1}^{+\infty} \hat{e}_2^{n-1}(0,l)(-\nu_2\lambda_2(l) + \nu_2\lambda_2(p))\phi_l(y),$$
$$\sum_{l=1}^{+\infty} \hat{e}_2^n(0,l)(-\nu_2\lambda_2(l) - \nu_1\lambda_1(q))\phi_l(y) = \sum_{i=1}^{+\infty} \hat{e}_1^{n-1}(0,i)(\nu_1\lambda_1(i) - \nu_1\lambda_1(q))\psi_i(y).$$

We truncate the expansions for $i, l > N$, since higher frequencies are not represented by the numerical grid, and we project the first equation onto ψ_k with respect to the scalar product $\langle\cdot,\cdot\rangle$ and the second one onto ϕ_j with respect to the weighted scalar product $\langle\cdot,\cdot\rangle_{\rm w}$,

(3.8)
$$\begin{aligned}\hat{e}_1^n(0,k)(\nu_1\lambda_1(k) + \nu_2\lambda_2(p)) &= \sum_{l=1}^{N} \hat{e}_2^{n-1}(0,l)(-\nu_2\lambda_2(l) + \nu_2\lambda_2(p))\langle\psi_k, \phi_l\rangle,\\ \hat{e}_2^n(0,j)(-\nu_2\lambda_2(j) - \nu_1\lambda_1(q)) &= \sum_{i=1}^{N} \hat{e}_1^{n-1}(0,i)(\nu_1\lambda_1(i) - \nu_1\lambda_1(q))\langle\phi_j, \psi_i\rangle_{\rm w}.\end{aligned}$$

Defining now the vectors $\mathbf{e}_j^n \in \mathbb{R}^N$ such that $(\mathbf{e}_j^n)_i := \hat{e}_j^n(0,i)$ for $j = 1, 2$, the matrices $V_{k,l} := \langle\psi_k, \phi_l\rangle$, $W_{j,i} := \langle\phi_j, \psi_i\rangle_{\rm w}$ and the diagonal matrices $(D_1)_{l,l} := (-\nu_2\lambda_2(l) + \nu_2\lambda_2(p)), (\tilde{D}_1)_{k,k} := (\nu_1\lambda_1(k) + \nu_2\lambda_2(p)), (D_2)_{i,i} := (\nu_1\lambda_1(i) - \nu_1\lambda_1(q)), (\tilde{D}_2)_{j,j} := (-\nu_2\lambda_2(j) - \nu_1\lambda_1(q))$, we obtain,

$$\begin{aligned}\mathbf{e}_1^n &= \tilde{D}_1^{-1}VD_1\mathbf{e}_2^{n-1},\\ \mathbf{e}_2^n &= \tilde{D}_2^{-1}WD_2\mathbf{e}_1^{n-1},\end{aligned} \tag{3.9}$$

which implies

$$\mathbf{e}_1^n = \tilde{D}_1^{-1}VD_1\tilde{D}_2^{-1}WD_2\mathbf{e}_1^{n-2} \quad \text{and} \quad \mathbf{e}_2^n = \tilde{D}_2^{-1}WD_2\tilde{D}_1^{-1}VD_1\mathbf{e}_2^{n-2}. \tag{3.10}$$

Since for two given matrices A, B the spectral radius satisfies $\rho(AB) = \rho(BA)$, we conclude that $\rho(\tilde{D}_1^{-1}VD_1\tilde{D}_2^{-1}WD_2) = \rho(\tilde{D}_2^{-1}WD_2\tilde{D}_1^{-1}VD_1)$ and, therefore, in order to accelerate the method, we are interested in the minimization problem

$$\min_{p,q\in\mathbb{R}} \rho((\tilde{D}_1^{-1}VD_1\tilde{D}_2^{-1}WD_2)(p,q)). \tag{3.11}$$

Problem (3.11) does not have yet a closed formula solution. However in the next section we show its efficiency by solving numerically the minimization problem.

Remark 3.5. Equation (3.11) is a straight generalization of the min-max problem (2.8). Indeed, assuming that the functions ψ_k and ϕ_j are orthogonal, the matrices V and W are the identity matrix. Therefore, (3.10) simplifies to $\mathbf{e}_1^n = \bar{D}\mathbf{e}_1^{n-2}$ and $\mathbf{e}_2^n = \bar{D}\mathbf{e}_2^{n-2}$, where the diagonal matrix $\bar{D}$ satisfies $(\bar{D})_{k,k} = \frac{\nu_2\lambda_2(k)-\nu_2\lambda_2(p)}{\nu_1\lambda_1(k)+\nu_2\lambda_2(p)}\frac{\nu_1\lambda_1(k)-\nu_1\lambda_1(q)}{\nu_2\lambda_2(k)+\nu_1\lambda_1(q)}$. Since the eigenvalues of a diagonal matrix are its diagonal entries we get that if $W = V = I$,

$$\min_{p,q\in\mathbb{R}} \rho((\tilde{D}_1^{-1}VD_1\tilde{D}_2^{-1}WD_2)(p,q)) = \min_{p,q}\max_k \left|\frac{\nu_2\lambda_2(k) - \nu_2\lambda_2(p)}{\nu_1\lambda_1(k) + \nu_2\lambda_2(p)}\frac{\nu_1\lambda_1(k) - \nu_1\lambda_1(q)}{\nu_2\lambda_2(k) + \nu_1\lambda_1(q)}\right|.$$

TABLE 2
Asymptotic behavior as $h \to 0$ for the reaction diffusion-diffusion coupling. Physical parameters: left table $\tilde{\eta}^2 = \lambda = 1$, right table $\tilde{\eta}^2 = \lambda = 10$.

h	ρ single sided	ρ double sided
1/50	0.7035	0.4052
1/100	0.7801	0.4748
1/500	0.8950	0.6160
1/1000	0.9245	0.6672
1/5000	0.9655	0.7650

h	ρ single sided	ρ double sided
1/50	0.1721	0.0337
1/100	0.2625	0.0456
1/500	0.4868	0.0685
1/1000	0.5823	0.0760
1/5000	0.7662	0.0872

Remark 3.6. The case of an arbitrary advection, i.e., $a_1 \neq 0$ and $a_2 \neq 0$ has been recently treated in [18] for homogeneous problems. Considering a heterogeneous problem with advection fields $\mathbf{a}_j = (a_{1j}, a_{2j})^\top$ in domain Ω_j, $j = 1, 2$, a separation of variables approach would lead to nonorthogonal functions $\psi_k(y) = e^{\frac{a_{21}y}{2\nu_1}} \sin(ky)$ and $\phi_k(y) = e^{\frac{a_{22}y}{2\nu_2}} \sin(ky)$ unless $\frac{a_{21}}{2\nu_1} = \frac{a_{22}}{2\nu_2}$, and thus it is not possible to obtain a recurrence relation as shown in (2.4) and (2.5). However, the approach developed in this section can be readily applied. The subdomain solutions are

$$e_1^n(x,y) = \sum_{k\in\mathcal{V}} \hat{e}_{1,k}^n e^{\frac{a_{21}y}{2\nu_1}} \sin(ky) e^{\lambda_1(k)x}, \quad e_2^n(x,y) = \sum_{k\in\mathcal{V}} \hat{e}_{2,k}^n e^{\frac{a_{22}y}{2\nu_2}} \sin(ky) e^{-\lambda_2(k)x},$$

with $\lambda_1(k) = \frac{a_{11}+\sqrt{4\nu_1^2k^2+4\nu_1^2\tilde{\eta_1}^2+a_{11}^2+a_{21}^2}}{2\nu_1}$ and $\lambda_2(k) = \frac{-a_{12}+\sqrt{4\nu_2^2k^2+4\nu_2^2\tilde{\eta_2}^2+a_{12}^2+a_{22}^2}}{2\nu_2}$. Defining $S_1 = \nu_2\lambda_2(p) + a_{12}$, $S_2 = \nu_1\lambda_1(p) - a_{11}$, the two scalar products $\langle f, g\rangle_{\mathrm{w}_1} = \frac{2}{L}\int_\Gamma f g e^{-\frac{a_{21}y}{\nu_1}} dy$ and $\langle f, g\rangle_{\mathrm{w}_2} = \frac{2}{L}\int_\Gamma f g e^{-\frac{a_{22}y}{\nu_2}} dy$, and repeating the calculations (3.7)–(3.9), one finds the recurrence relation (3.10), with $V_{k,l} := \langle \psi_k, \phi_l\rangle_{\mathrm{w}_1}$, $W_{j,i} := \langle \phi_j, \psi_i\rangle_{\mathrm{w}_2}$, and the diagonal matrices $(D_1)_{l,l} := (-\nu_2\lambda_2(l) + \nu_2\lambda_2(p))$, $(\tilde{D}_1)_{k,k} := (\nu_1\lambda_1(k) + \nu_2\lambda_2(p) - a_{11} + a_{12})$, $(D_2)_{i,i} := (\nu_1\lambda_1(i) - \nu_1\lambda_1(q))$, $(\tilde{D}_2)_{j,j} := (-\nu_2\lambda_2(j) - \nu_1\lambda_1(q) - a_{12} + a_{11})$.

4. Numerical results. Our numerical experiments to test the different coupling strategies separately are performed using the subdomains $\Omega_1 = (-1, 0) \times (0, 1)$, $\Omega_2 = (0, 1) \times (0, 1)$. We use a classical five point finite difference scheme for the interior points and treat the normal derivatives with second order discretization using a ghost point formulation.

4.1. Reaction diffusion-diffusion coupling. We first consider the reaction diffusion-diffusion coupling analyzed in section 2. Tables 2 and 3 show the values of the convergence factor in two different asymptotic regimes, when $h \to 0$ and for strong heterogeneity. As the asymptotic Theorem 2.11 and Remark 2.5 state, a strong heterogeneity improves the performance of the algorithm. In the single sided optimized case, the value of the convergence factor $|\rho(k)|$ tends to 1, while in the double sided case, $|\rho(k)|$ is bounded either by λ or by $1/\lambda$. Figure 4 shows the number of iterations required to reach convergence with a tolerance of 10^{-6} as function of the optimized parameters in both the single and double sided cases. We see that the analysis predicts the optimized parameter very well.

4.2. Advection reaction diffusion-diffusion coupling. Next, we consider the advection reaction diffusion-diffusion coupling with advection normal to the interface. Table 4 summarizes the behavior of $\rho(k)$ as $h \to 0$ and for strong heterogeneity. Similarly, Figure 5 shows the number of iterations required to reach convergence with the tolerance of 10^{-6}. Figure 6 shows the number of iterations to reach conver-

TABLE 3
Asymptotic behavior as $\lambda \to 0$ and $\lambda \to \infty$, with $h = 0.05$ for the reaction diffusion-diffusion coupling. Physical parameter: $\tilde{\eta}^2 = 1$.

λ	ρ single sided	ρ double sided
0.001	0.0125	$7.8 \cdot 10^{-4}$
0.01	0.1075	0.0078
0.1	0.4453	0.0757
1	0.5851	0.4748
10	0.2625	0.076
100	0.0389	0.0078
1000	0.0040	$7.8 \cdot 10^{-4}$

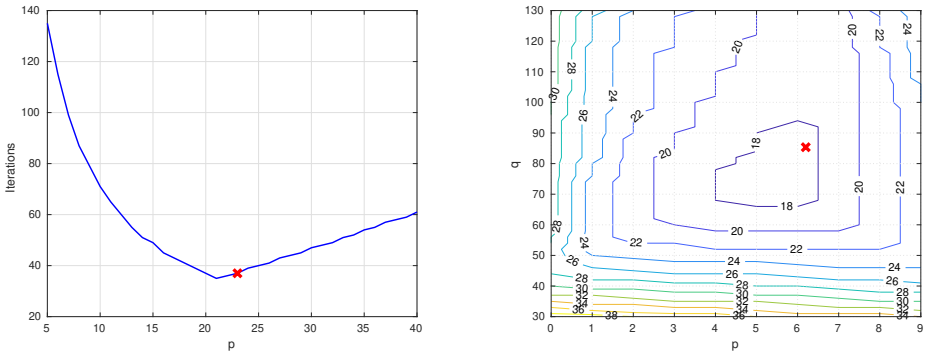

FIG. 4. *Number of iterations required to reach convergence with a tolerance of 10^{-6} as function of the optimized parameters for the reaction diffusion-diffusion coupling. The left panel shows the single sided case while the right panel shows the double sided case. Physical parameters: $\nu_1 = 2$, $\nu_2 = 1$, $\eta^2 = 10$, mesh size $h = 0.02$.*

gence for the tangential advection case. The minimization problem (3.11) is solved numerically to find the optimal parameters p and q using the Nelder–Mead algorithm. We have solved the minimization problem with different initial couples (p, q) and we have noticed that the optimal solution satisfies an ordering relation between p and q depending on λ as in Theorems 2.11 and 3.4.

4.3. Application to the contaminant transport problem. The computational domain Ω described in Figure 1 is set equal to $\Omega = (0, 8) \times (-4, 0)$, with $\Omega_j = (0, 8) \times (1 - j, -j)$, $j = 1, \ldots, 4$. On the top boundary Γ_1, we impose a condition on the incoming contaminant flow, i.e., $\frac{\partial u}{\partial y} - a_2 u = 1$ while on the bottom edge Γ_3 we impose a zero Neumann boundary condition $\frac{\partial u}{\partial y} = 0$. On the vertical edges Γ_2 and Γ_4 we set absorbing boundary conditions so that

$$\begin{aligned} \tfrac{\partial u}{\partial \mathbf{n}} + pu = 0 \quad &\text{on} \quad \{0\} \times [-3; 0] \text{ and } \{8\} \times [-3; 0], \\ \tfrac{\partial u}{\partial \mathbf{n}} - a_1 u + pu = 0 \quad &\text{on} \quad \{0\} \times [-4; -3] \text{ and } \{8\} \times [-4; -3], \end{aligned}$$

where $\mathbf{n}$ is the outgoing normal vector. The parameter p is chosen equal to $p = \sqrt{\pi \frac{\pi}{h}}$, being $k_{\min} = \pi$ and $k_{\max} = \frac{\pi}{h}$. This choice derives from the observation that imposing $\frac{\partial u}{\partial n} + DtNu = 0$, where DtN is the Dirichlet to Neumann operator, is an exact transparent boundary condition; see [29, 28]. Thus we replace the expensive exact transparent boundary condition with an approximation of the DtN operator. We know from [9] that $p = \sqrt{\pi \frac{\pi}{h}}$ is indeed a zero order approximation of the DtN

TABLE 4

For the advection reaction diffusion-diffusion coupling, the left table shows the asymptotic behaviour when $h \to 0$ while the right table shows the values of the convergence factor for strong heterogeneity when $h = 1/50$. Physical parameters: $\eta_1^2 = 1, \eta_2^2 = 2, \nu_1 = 2, \nu_2 = 1, a_2 = 0$, $a_1 = 5$, mesh size $h = 0.02$.

h	ρ single sided	ρ double sided
1/50	0.4766	0.1835
1/100	0.5910	0.2306
1/500	0.7889	0.3274
1/1000	0.8452	0.3618
1/5000	0.9273	0.4228

λ	ρ single sided	ρ double sided
0.001	0.0031	$4.89 \cdot 10^{-4}$
0.01	0.0297	0.0049
0.1	0.2101	0.0458
1	0.4865	0.2552
10	0.2786	0.0517
100	0.0459	0.0056
1000	0.0049	$5.6 \cdot 10^{-4}$

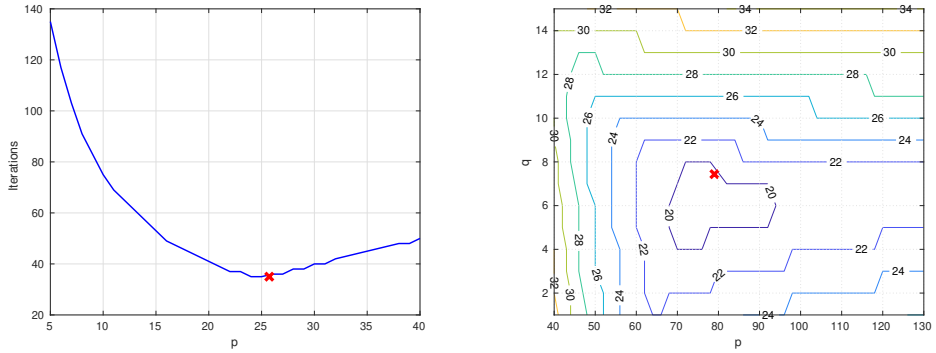

FIG. 5. *Number of iterations required to reach convergence with a tolerance of 10^{-6} as function of the optimized parameters for the advection reaction diffusion-diffusion coupling with normal advection. Physical parameters: $\nu_1 = 2$, $\nu_2 = 1$, $\eta_1^2 = 1$, $\eta_2^2 = 2, a_1 = 5$, mesh size $h = 0.02$.*

operator. To solve the system of PDEs, we consider the optimized Schwarz method:

(4.1)

$$
\begin{aligned}
-\nu_1 \Delta u_1^n - a_2 \partial_y u_1^n &= 0 && \text{in } \Omega_1, && \mathcal{B}_1(u_1^n) = 0 \text{ on } \partial\Omega_1 \setminus \Sigma_1,\\
\partial_{n_{1,2}} u_1^n + p_{12} u_1^n &= \partial_{n_{1,2}} u_2^{n-1} + p_{12} u_2^{n-1} && \text{on } \Sigma_1,\\
\eta_2^2 u_2^n - \nu_2 \Delta u_2^n &= 0 && \text{in } \Omega_2, && \mathcal{B}_2(u_2^n) = 0 \text{ on } \partial\Omega_2 \setminus \{\Sigma_1, \Sigma_2\},\\
\partial_{n_{1,1}} u_2^n + p_{21} u_2^n &= \partial_{n_{1,1}} u_1^{n-1} + p_{21} u_1^{n-1} && \text{on } \Sigma_1,\\
\partial_{n_{2,3}} u_2^n + p_{23} u_2^n &= \partial_{n_{2,3}} u_3^{n-1} + p_{23} u_3^{n-1} && \text{on } \Sigma_2,\\
-\nu_3 \Delta u_3^n &= 0 && \text{in } \Omega_3, && \mathcal{B}_3(u_3^n) = 0 \text{ on } \partial\Omega_3 \setminus \{\Sigma_2, \Sigma_3\},\\
\partial_{n_{2,2}} u_3^n + p_{32} u_3^n &= \partial_{n_{2,2}} u_2^{n-1} + p_{32} u_2^{n-1} && \text{on } \Sigma_2,\\
\partial_{n_{3,4}} u_3^n + p_{34} u_3^n &= \partial_{n_{3,4}} u_4^{n-1} + p_{34} u_4^{n-1} && \text{on } \Sigma_3,\\
-\nu_4 \Delta u_4^n + a_1 \partial_x u_4^n &= 0 && \text{in } \Omega_4, && \mathcal{B}_4(u_4^n) = 0 \text{ on } \partial\Omega_4 \setminus \Sigma_3,\\
\partial_{n_{3,3}} u_4^n + p_{43} u_4^n &= \partial_{n_{3,3}} u_3^{n-1} + p_{43} u_3^{n-1} && \text{on } \Sigma_3,
\end{aligned}
$$

where Σ_i are the shared interfaces $\Sigma_i = \partial\Omega_i \cap \partial\Omega_{i+1}, i = 1, 2, 3$, the vectors $\mathbf{n}_{i,j}$ are the normal vectors on the interface Σ_i pointing towards the interior of the domain Ω_j, and the operators $\mathcal{B}_i(u_i)$ represent the boundary conditions to impose on the boundary excluding the shared interfaces. Regarding the Robin parameters $p_{i,j}$, we choose them according to the two subdomain analysis carried out in this manuscript. Due to the exponential decay of the error away from the interface (see eq. (2.3)), if the subdomains are not too narrow in the y direction, the information transmitted from each subdomain to the neighboring one does not change significantly and, therefore,

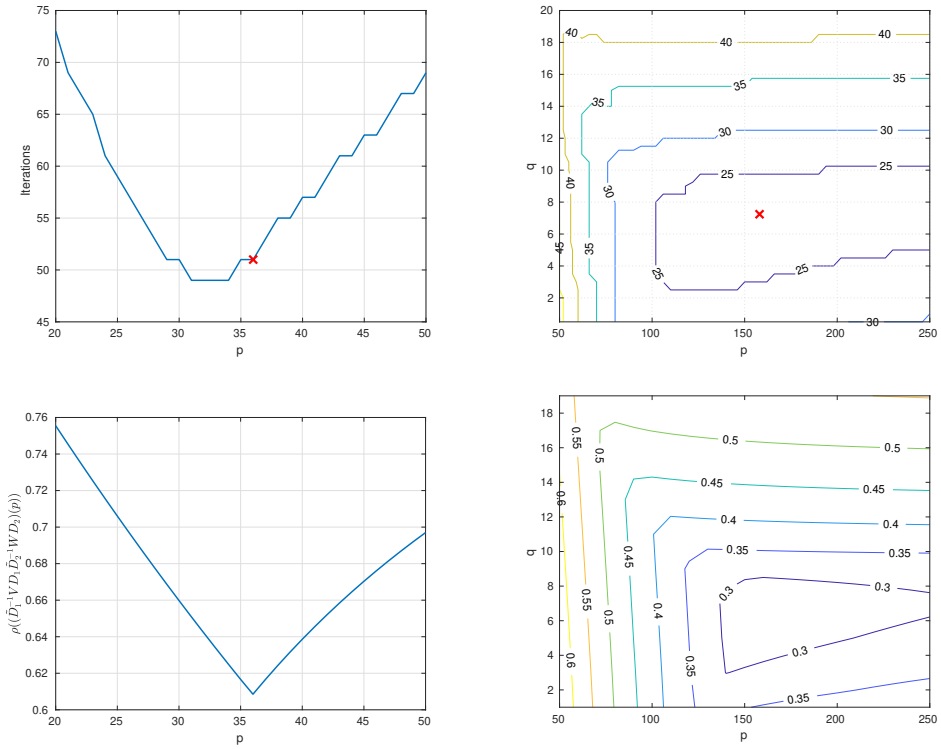

FIG. 6. *In the top row, we show the number of iterations required to reach convergence with a tolerance of* 10^{-6} *as function of the optimized parameters for the advection reaction diffusion-diffusion coupling with tangential advection. In the bottom row, we show the dependence on* p *and the level curves of the objective function in the min-max problem* (3.11). *Physical parameters:* $\nu_1 = 1$, $\nu_2 = 2$, $\eta_1^2 = 1$, $\eta_2^2 = 2, a_2 = 15$, *mesh size* $h = 0.01$.

the $p_{i,j}$ from a two subdomain analysis are still a good choice. We remark that this argument does not hold for the Helmholtz equation, for which there are resonant modes for frequencies $k \leq \omega$, where ω is the wave number, which travel along the domains and they do not decay away from the interface. Figure 7 shows the stationary distribution of the contaminant. We observe that due to the advection in the y direction in Ω_1, the contaminant accumulates on the interface with Ω_2, representing the porous medium, and here we have the highest concentration. Then the contaminant diffuses into the layers below and already in the porous media region it feels the presence of the tangential advection in Ω_4. Next, we also consider the transient version of (4.1). We discretize the time derivative with an implicit Euler scheme, so that each equation has a further reaction term equal to $\eta_{j,tran}^2 = \eta_{j,stat}^2 + \frac{1}{\Delta t}$. Figure 8 shows the time dependent evolution of the concentration u over 400 integration steps. The initial condition is set equal to zero on the whole domain Ω.

Table 5 shows the number of iterations to reach a tolerance of 10^{-6} for the algorithm (4.1) both used as an iterative method and as a preconditioner for GMRES for the substructured system; see [13] for an introduction to the substructured version of (4.1). We consider both single and double sided optimizations for the parameters $p_{i,j}$

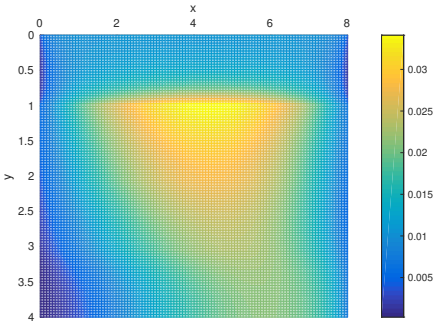

FIG. 7. *Stationary distribution of the contaminant. Physical parameters:* $\nu_1 = 0.5, \nu_2 = 3, \nu_3 = 3, \nu_4 = 1, \eta_2^2 = 0.01, a_2 = 2, a_1 = 2$.

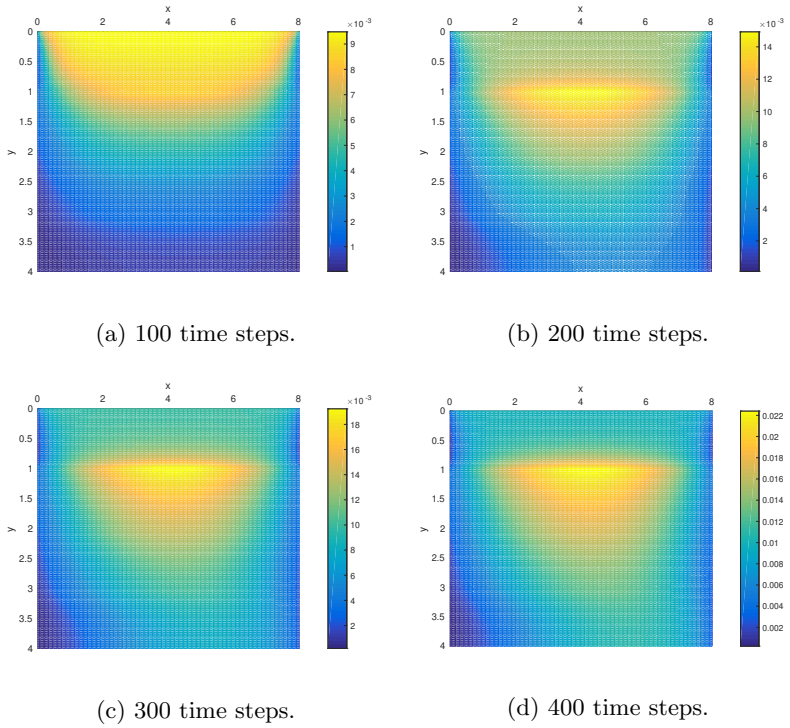

(a) 100 time steps.

(b) 200 time steps.

(c) 300 time steps.

(d) 400 time steps.

FIG. 8. *Evolution of the contaminant concentration* u.

at each interface. For the time evolution problem, the stopping criterion is

$$\max\left\{\frac{\|u_{1,\Sigma_1}^{n,k} - u_{2,\Sigma_1}^{n,k}\|}{\|u_{1,\Sigma_1}^{n,k}\|}, \frac{\|u_{2,\Sigma_2}^{n,k} - u_{3,\Sigma_2}^{n,k}\|}{\|u_{2,\Sigma_2}^{n,k}\|}, \frac{\|u_{3,\Sigma_1}^{n,k} - u_{4,\Sigma_3}^{n,k}\|}{\|u_{3,\Sigma_3}^{n,k}\|}\right\} \leq 10^{-6}. \tag{4.2}$$

From Figures 7 and 8, we note that this physical configuration would represent a safe situation since a very small concentration of contaminant manages to get through the vertical diffusive layers and reaches the right-bottom of the domain, where it could pollute the water well.

TABLE 5

Number of iterations to reach a tolerance of 10^{-6} *for the optimized Schwarz method* (4.1) *used as an iterative method and as a preconditioner. The left side refers to the stationary case while the right side to the transient one where we consider the number of iterations needed to satisfy the stopping criterion* (4.2) *averaged over* 400 *time steps.*

	Iterative	GMRES
Single sided	270	33
Double sided	55	25

	Iterative	GMRES
Single sided	11.5	5.7
Double sided	9.6	4.3

5. Conclusions. In this manuscript we considered the heterogeneous couplings arising from second order elliptic PDEs and solved analytically the corresponding min-max problems, except in the case of tangential advection to the interface where we provided a numerical optimization procedure. Our results show that optimized Schwarz methods are not only natural for heterogeneous problems, they are also extremely efficient. Indeed, the asymptotic analysis shows that the stronger the heterogeneity is, the faster becomes the convergence. In particular, a double sided method should be preferred since not only is it clearly faster than a single sided one, but it also leads to an h independent convergence as long as there is a jump in the diffusion coefficients. Our analysis is based on a two-dimensional setting but the results can be extended to three-dimensional problems. Considering $\Omega_1 = (-\infty, 0) \times (0, L) \times (0, \hat{L})$ and $\Omega_2 = (0, +\infty) \times (0, L) \times (0, \hat{L})$, we can obtain analogous sine expansions for the errors e_j^n, $j = 1, 2$ as in section 2. Then, for symmetric problems and in the case of normal advection to the plane $\Gamma := \{0\} \times (0, L) \times (0, \hat{L})$, we can reuse the same theoretical results by changing the range of frequencies in the min-max problems, setting $k_{\min} = \frac{\pi}{L} + \frac{\pi}{\hat{L}}$ and $k_{\max} = \frac{2\pi}{h}$. Considering tangential advection, all of the possible tangential directions now lie on the plane Γ, which in our example is the y-z plane. Then one could use the numerical procedure developed in section 3.3 introducing the matrices V and W and proper scalar products defined as integrals on the two-dimensional interface.

REFERENCES

[1] J. BEAR AND A. CHENG, *Modeling Groundwater Flow and Contaminant Transport*, Theory and Applications of Transport in Porous Media, Springer, The Netherlands, 2010.

[2] N. BIRGLE, R. MASSON, AND L. TRENTY, *A domain decomposition method to couple nonisothermal compositional gas liquid Darcy and free gas flows*, J. Comput. Phys., 368 (2018), pp. 210–235.

[3] E. BLAYO, D. CHEREL, AND A. ROUSSEAU, *Towards optimized Schwarz methods for the Navier-Stokes equations*, J. Sci. Comput., 66 (2016), pp. 275–295.

[4] V. DOLEAN, M. J. GANDER, AND L. GERARDO-GIORDA, *Optimized Schwarz methods for Maxwell's equations*, SIAM J. Sci. Comput., 31 (2009), pp. 2193–2213, https://doi.org/10.1137/080728536.

[5] V. DOLEAN, M. J. GANDER, AND E. VENEROS, *Optimized Schwarz methods for Maxwell equations with discontinuous coefficients*, in Domain Decomposition Methods in Science and Engineering XXI, Lect. Notes Comput. Sci. Eng. 98, Springer, Cham, 2014, pp. 517–525.

[6] V. DOLEAN AND F. NATAF, *A new domain decomposition method for the compressible Euler equations*, M2AN Math. Model. Numer. Anal., 40 (2006), pp. 689–703.

[7] O. DUBOIS, *Optimized Schwarz Methods for the Advection-Diffusion Equation*, Ph.D. thesis, McGill University, Montreal, Quebec, Canada, 2007.

[8] O. DUBOIS, *Optimized Schwarz methods with Robin conditions for the advection-diffusion equation*, in Domain Decomposition Methods in Science and Engineering XVI, Lect. Notes Comput. Sci. Eng., 55, Springer, Berlin, 2007, pp. 181–188.

[9] M. J. GANDER, *Optimized Schwarz methods*, SIAM J. Numer. Anal., 44 (2006), pp. 699–731, https://doi.org/10.1137/S0036142903425409.

[10] M. J. Gander, *Schwarz methods over the course of time*, Electron. Trans. Numer. Anal., 31 (2008), pp. 228–255.
[11] M. J. Gander, *On the influence of geometry on optimized Schwarz methods*, SeMA J., 53 (2011), pp. 71–78.
[12] M. J. Gander and O. Dubois, *Optimized Schwarz methods for a diffusion problem with discontinuous coefficient*, Numer. Algorithms, 69 (2015), pp. 109–144.
[13] M. J. Gander and L. Halpern, *Méthodes de décomposition de domaine*, Encyclopédie électronique pour les ingénieurs, 2012.
[14] M. J. Gander, L. Halpern, and F. Magoules, *An optimized Schwarz method with two-sided Robin transmission conditions for the Helmholtz equation*, Internat. J. Numer. Methods Fluids, 55 (2007), pp. 163–175.
[15] M. J. Gander, L. Halpern, and V. Martin, *A new algorithm based on factorization for heterogeneous domain decomposition*, Numer. Algorithms, 73 (2016), pp. 167–195.
[16] M. J. Gander, F. Magoules, and F. Nataf, *Optimized Schwarz methods without overlap for the Helmholtz equation*, SIAM J. Sci. Comput., 24 (2002), pp. 38–60, https://doi.org/10.1137/S1064827501387012.
[17] M. J. Gander and T. Vanzan, *Heterogeneous optimized Schwarz methods for coupling Helmholtz and Laplace equations*, in Domain Decomposition Methods in Science and Engineering XXIV, Springer, Cham, 2018, pp. 311–320.
[18] M. J. Gander and T. Vanzan, *Optimized Schwarz methods for advection diffusion equations in bounded domains*, in Numerical Mathematics and Advanced Applications ENUMATH 2017, F. A. Radu, K. Kumar, I. Berre, J. M. Nordbotten, and I. S. Pop, eds., Springer, Cham, 2019, pp. 921–929.
[19] M. J. Gander and Y. Xu, *Optimized Schwarz methods for model problems with continuously variable coefficients*, SIAM J. Sci. Comput., 38 (2016), pp. A2964–A2986, https://doi.org/10.1137/15M1053943.
[20] M. J. Gander and Y. Xu, *Optimized Schwarz methods with nonoverlapping circular domain decomposition*, Math. Comp., 86 (2017), pp. 637–660.
[21] L. Gerardo-Giorda, F. Nobile, and C. Vergara, *Analysis and optimization of Robin–Robin partitioned procedures in fluid-structure interaction problems*, SIAM J. Numer. Anal., 48 (2010), pp. 2091–2116, https://doi.org/10.1137/09076605X.
[22] S.-C. Lee, M. N. Vouvakis, and J.-F. Lee, *A non-overlapping domain decomposition method with non-matching grids for modeling large finite antenna arrays*, J. Comput. Phys., 203 (2005), pp. 1–21.
[23] F. Lemarié, L. Debreu, and E. Blayo, *Toward an Optimized Global-in-Time Schwarz Algorithm for Diffusion Equations with Discontinuous and Spatially Variable Coefficients, Part 1: The Constant Coefficients Case*, Electron. Trans. Numer. Anal., 40 (2013), pp. 148–169.
[24] F. Lemarié, L. Debreu, and E. Blayo, *Toward an Optimized Global-in-Time Schwarz Algorithm for Diffusion Equations with Discontinuous and Spatially Variable Coefficients, Part 2: The Variable Coefficients Case*, Electron. Trans. Numer. Anal., 40 (2013), pp. 170–186.
[25] P.-L. Lions, *On the Schwarz Alternating Method* III*: A Variant for Nonoverlapping Subdomains*, in Proceedings of the Third International Symposium on Domain Decomposition Methods for Partial Differential Equations, SIAM, Philadelphia, 1990, pp. 202–223.
[26] Y. Maday and F. Magoulés, *Optimized Schwarz methods without overlap for highly heterogeneous media*, Comput. Methods Appl. Mech. Engrg., 196 (2007), pp. 1541–1553.
[27] V. Martin, *Schwarz waveform relaxation method for the viscous shallow water equations*, in Domain Decomposition Methods in Science and Engineering, Lect. Notes Comput. Sci. Eng. 40, Springer, Berlin, pp. 653–660.
[28] F. Nataf, *Absorbing boundary conditions and perfectly matched layers in wave propagation problems*, in Direct and Inverse Problems in Wave Propagation and Applications, Radon Ser. Comput. Appl. Math. 14, De Gruyter, Berlin, 2013, pp. 219–232.
[29] F. Nataf, F. Rogier, and E. De Sturler, *Optimal Interface Conditions for Domain Decomposition Methods*, Tech. report, Ecole Polytechnique, Paris, France, 1994.
[30] Z. Peng and J.-F. Lee, *A scalable nonoverlapping and nonconformal domain decomposition method for solving time-harmonic Maxwell equations in r^3*, SIAM J. Sci. Comput., 34 (2012), pp. A1266–A1295, https://doi.org/10.1137/100817978.
[31] A. Quarteroni and A. Valli, *Domain Decomposition Methods for Partial Differential Equations*, Numerical Mathematics and Science, Clarendon Press, Oxford University Press, New York, 1999.
[32] P. Tchebychev, *Théorie des mécanismes connus sous le nom de parallélogrammes*, Imprimerie de l'Académie impériale des sciences, 1853.